Quaternary Science Reviews 229 (2020) 106091

Contents lists available at ScienceDirect

Quaternary Science Reviews

journal homepage: www.elsevier.com/locate/quascirev

Deglaciation of the Greenland and Laurentide ice sheets interrupted by glacier advance during abrupt coolings

Nicolás E. Young [a, *], Jason P. Briner [b], Gifford H. Miller [c], Alia J. Lesnek [b], Sarah E. Crump [c], Elizabeth K. Thomas [b], Simon L. Pendleton [c], Joshua Cuzzone [d], Jennifer Lamp [a], Susan Zimmerman [e], Marc Caffee [f, g], Joerg M. Schaefer [a]

[a] Lamont-Doherty Earth Observatory, Columbia University, Palisades, NY, USA
[b] Department of Geology, University at Buffalo, Buffalo, NY, USA
[c] INSTAAR and Department of Geological Sciences, University of Colorado Boulder, Boulder, CO, USA
[d] Department of Earth System Science, University of California Irvine, Irvine, CA, USA
[e] Lawrence Livermore National Laboratory, Center for Accelerator Mass Spectrometry, Livermore, CA, USA
[f] Department of Physics, PRIME Lab, Purdue University, West Lafayette, IN, USA
[g] Department of Earth, Atmospheric, and Planetary Science, Purdue University, West Lafayette, IN, USA

ARTICLE INFO

Article history:
Received 1 November 2019
Accepted 19 November 2019
Available online xxx

ABSTRACT

Understanding patterns of ice-sheet deglaciation is key for predicting the rate of future ice-sheet melt, yet the processes underlying deglaciation remain elusive. The early Holocene (11.7 ka to 8.2 ka; Greenlandian Stage) represents the most recent period when the Laurentide and Greenland ice sheets underwent large-scale recession. Moreover, this ice-sheet recession occurred under the backdrop of regional temperatures that were similar to or warmer than today, and comparable to those projected for the upcoming centuries. Reconstructing Laurentide and Greenland ice sheet behavior during the early Holocene, and elucidating the mechanisms dictating this behavior may serve as a partial analog for future Greenland ice-sheet change in a warming world. Here, we present 123 new ^{10}Be surface exposure ages from two sites on Baffin Island and southwestern Greenland that constrain the behavior of the Laurentide and Greenland ice sheets, and an independent alpine glacier during the early Holocene. On Baffin Island, we focus on a unique area where moraines deposited by the Laurentide Ice Sheet rest directly adjacent to moraines deposited by an independent alpine glacier. Sixty-one ^{10}Be ages reveal that advances and/or stillstands of the Laurentide Ice Sheet and an alpine glacier occurred in unison around 11.8 ka, 10.3 ka, and 9.2 ka. Sixty-two ^{10}Be ages from southwestern Greenland indicate that the Greenland Ice Sheet margin experienced re-advances or stillstands around 11.6 ka, 10.4 ka, 9.1 ka, 8.1 ka, and 7.3 ka. Our results reveal that ice sheets respond to climate perturbations on the same centennial timescale as small alpine glaciers. We hypothesize that during the warming climate of the early Holocene, freshening of the North Atlantic Ocean induced by ice-sheet melt resulted in regional cooling and brief periods of ice-sheet stabilization superimposed on net glacier recession. These observations point to a negative feedback mechanism inherent to melting ice sheets in the Baffin Bay region that slows ice-sheet recession during intervals of otherwise rapid deglaciation.

© 2019 Elsevier Ltd. All rights reserved.

1. Introduction

The early Holocene in the North Atlantic region was characterized by a warming climate when temperatures were similar to or exceeded modern (e.g. Briner et al., 2016; Pendleton et al., 2019). The general warmth of the early Holocene, however, was punctuated by abrupt, multi-decadal to centennial-scale cooling events that likely involved alteration of Atlantic Meridional Overturning Circulation (AMOC) driven by freshwater input into the North Atlantic Ocean via rapidly melting ice sheets (Thornalley et al., 2009; Renssen et al., 2009). The most widespread and therefore well-known of these cooling events occurred ca. 9.3 and 8.2 ka (Alley et al., 1997; Barber et al., 1999; Yu et al., 2010), but several additional freshwater events in the North Atlantic region likely

* Corresponding author.
E-mail address: nicolasy@ldeo.columbia.edu (N.E. Young).

https://doi.org/10.1016/j.quascirev.2019.106091
0277-3791/© 2019 Elsevier Ltd. All rights reserved.

occurred during the early Holocene (Jennings et al., 2015). Characterizing the behavior of the Laurentide and Greenland ice sheets (LIS and GrIS) during the early Holocene provides key insights into how these ice sheets retreat in a warming climate, the timescales at which these ice sheets might respond to climate, their role in AMOC-driven climate change, and the potential of the modern Greenland Ice Sheet to drive and/or respond to AMOC-driven climate change.

During the last glaciation most of the currently ice-free fringe that surrounds Baffin Bay was covered by the Laurentide and Greenland ice sheets (Fig. 1). Following the Last Glacial Maximum (LGM; ~26–19.5 ka; Clark et al., 2009), net retreat of the LIS and GrIS was interrupted by numerous ice sheet re-advances or still-stands, the evidence for which can currently be found along the continental margins surrounding Baffin Bay. On Baffin Island, Arctic Canada, a series of moraines delimit the former margins of the LIS as it retreated out of Baffin Bay towards what is now the Barnes Ice Cap (Fig. 1; Falconer et al., 1965; Andrews and Ives, 1978). In southwestern Greenland, distinct moraine systems were deposited as the GrIS retreated eastwards out of Baffin Bay and towards the present GrIS configuration (Fig. 1; Weidick, 1968, 1974). The age of deposition of these moraine systems on Baffin Island and southwestern Greenland has long been assigned to the early Holocene based largely on the loose association with radiocarbon-dated marine deposits (e.g. Andrews and Ives, 1978; Ten Brink, 1975). Yet, the low temporal resolution of these moraine chronologies prevents a critical assessment of the mechanisms causing moraine deposition during the deglaciation. Was moraine deposition forced by stochastic processes, or did Holocene climate variability drive a pattern of moraine deposition imprinted on large-scale net ice-sheet recession?

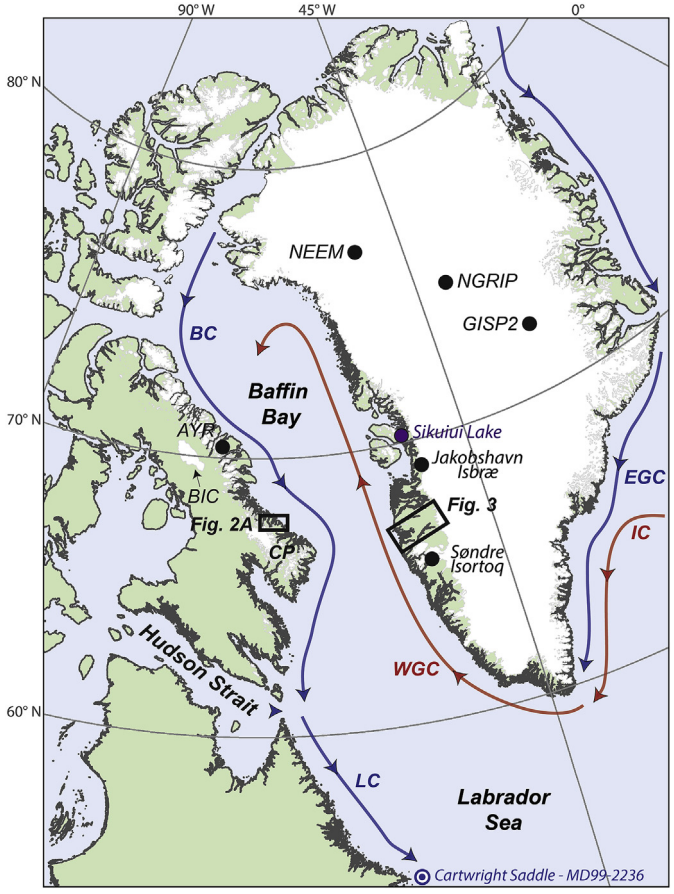

Fig. 1. Baffin Bay region with locations discussed in the text. AYR – Ayr Lake, BIC – Barnes Ice Cap, CP – Cumberland Peninsula, BC – Baffin Current, LC – Labrador Current, WGC – West Greenland Current, IC – Irminger Current, EGC – East Greenland Current.

In this paper, we describe an extensive effort to characterize, in detail, the early Holocene behavior of the Baffin Bay margins of the LIS and GrIS, and an independent alpine glacier. We present 123 new ^{10}Be ages from two sites in Baffin Bay, located on Baffin Island and southwestern Greenland (Fig. 1). On Baffin Island, we selected a unique field site where moraines deposited by two LIS outlet glaciers rest directly adjacent to moraines deposited by an independent alpine glacier. This allows us to reconstruct the response of two independent ice masses of varying size to the same climate forcing. In southwestern Greenland, we reconstruct the timing of eastward retreat of the GrIS across what is presently Greenland's largest ice-free land area (Fig. 1). We combine these datasets to address the following questions: 1) do ice sheets and alpine glaciers respond to climate forcing on the same time scale? 2) are patterns of early Holocene ice-sheet recession consistent between the LIS and GrIS, or are there key differences? 3) did known short-lived cooling events in the early Holocene affect patterns of ice-sheet recession, 4) what role, if any, did the LIS and GrIS play in forcing these abrupt cooling events, and 5) broadly, do ice sheets react abruptly to multi-decadal to centennial-scale climate forcing, or are millennial-scale climate trends required to elicit a significant ice-sheet response?

2. Deglaciation of Baffin Island and the King Harvest site, Cumberland Peninsula

During the LGM, alpine glaciers merged with major LIS outlet glaciers on Baffin Island, with maximum LGM ice extending to at least the outer eastern coast and perhaps out onto the continental shelf (Miller et al., 2002; Kaplan and Miller, 2003; Dyke, 2004; Briner et al., 2006) During deglaciation, eventual separation of LIS and alpine ice allowed each to independently deposit a series of moraines across Baffin Island, generally referred to as the Cockburn Moraines (Andrews and Ives, 1978). The outermost Cockburn Moraines were originally mapped as the late Wisconsin maximum extent of alpine glaciers and the LIS (Falconer et al., 1965); however, subsequent work has revealed that Cockburn Moraines were deposited during overall ice recession long after the classic LGM. Cockburn moraines are broadly centered at the heads of fjords (LIS ice), and beyond the Little Ice Age/historical maximum moraine in alpine valleys (Andrews and Ives, 1978; Briner et al., 2009). Based on the geomorphic relationship between fossiliferous marine deposits and moraines, deposition of the Cockburn moraines is broadly and indirectly constrained with radiocarbon to between ~9.5 ka and 8.5 ka (Briner et al., 2009). In one location, mapped Cockburn moraines deposited by alpine glaciers have been directly dated with ^{10}Be to ~8.2 ka (Young et al., 2012). Following deposition of the Cockburn moraines, continued retreat of the LIS culminated in what is now the Barnes Ice Cap, one of the last remaining vestiges of the LIS (Fig. 1).

Located in southern Baffin Island, the Cumberland Peninsula hosts the Penny Ice Cap, numerous smaller mountain ice caps and cirque glaciers, and deep fjords that once contained LIS outlet glaciers (Fig. 1; Fig. 2A). During the LGM, the Cumberland Peninsula was largely inundated with ice, with a few areas of the modern coastline, and perhaps some nunataks, remaining ice free as ice concentrated in fjords (Miller et al., 2002). Situated between Narpaing Fjord and Okoa Bay on the Cumberland Peninsula (Fig. 2A), the King Harvest field site (informal name) contains several small cirque glaciers that, when expanded, converge into one primary alpine glacier (Fig. 2B). At the mouth of the King Harvest valley lie

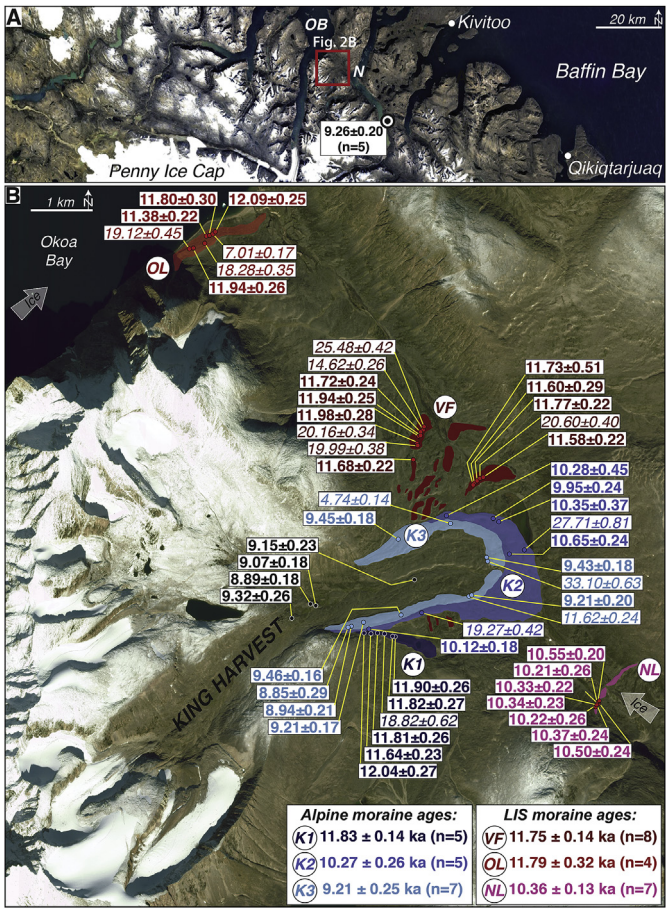

Fig. 2. (A) Study region on the Cumberland Peninsula, Baffin Island. OB – Okoa Bay, N – Narpaing Fjord. Bullseye marks the location of the up-fjord lateral moraine (Fig. 7). (B) King Harvest site located between Okoa Bay and Narpaing Fjord. OL – Okoa lateral moraine, VF – valley-floor moraine, NL – Narpaing lateral moraine. Individual ^{10}Be ages are presented in thousands of years with the 1-sigma analytical uncertainty only; outliers are in italics (Table 1; Figs. 7 and 8). The valley-floor moraine and the Narpaing lateral moraine were deposited by ice emanating from Narpaing Fjord (Fig. 4). K1–K3 are alpine moraines deposited by the King Harvest glacier system. Stated moraine ages are the arithmetic mean ± 1SD (Table 1).

well-defined lateral and end moraines resting directly next to moraines deposited by LIS outlet glaciers that once occupied Narpaing Fjord and Okoa Bay (Fig. 2B; Miller, 1973). Moraines preserved in the King Harvest region have classically been considered part of the Cockburn moraine system (Miller, 1973, Fig. 2B), and the uniqueness of the King Harvest moraine sequence where LIS moraines rest adjacent to alpine moraines in the same glacier forefield has long been recognized (Miller, 1973; Briner et al., 2009). Within a relatively restricted area, the King Harvest region provides access to moraine systems deposited by independent ice masses – independent ice masses that were influenced by the same climatic regime.

3. Southwestern Greenland ice sheet

During the LGM, the western margin of the GrIS extended beyond the modern coastline out onto the continental shelf (Fig. 1; Funder; Ó Cofaigh et al., 2013). However, it is unknown if the GrIS extended to the shelf edge or terminated somewhere on the inner shelf (Funder et al., 2011). Submerged moraines on the continental shelf include the Hellefisk (~100 km offshore) and Sisimiut moraine complexes (~20 km offshore), and have been tentatively assigned to the LGM and lateglacial period, respectively, but no direct age constraints exist (van Tatenhove et al., 1996; Funder et al., 2011). Recession of the GrIS within the modern coastline is thought to have occurred between ~11 and 10 cal ka BP based on several minimum-limiting coastal radiocarbon ages (Bennike and Björck, 2002) and in the immediate Sisimiut region, the oldest coastal radiocarbon age is ~10.8 cal ka BP (Bennike et al., 2011). Moreover, these age constraints serve as minimum-limiting ages for the offshore Hellefisk and Sisimiut moraine systems.

Quaternary surficial deposits on the landscape between the present coastline and modern ice margin were initially mapped in detail by Weidick (1974), and further refined by Ten Brink (1975) and van Tatenhove et al. (1996), and these efforts provide a firm foundation for which to characterize the recession of the GrIS. Following ice-sheet recession within the present coastline, the GrIS deposited a series of N–S trending moraines between the coastline and modern ice margin: Taserqat, Sarfartôq-Avatdelq, Fjord, Umîvît-Keglen, and Ørkendalen (Fig. 3; Weidick, 1974; van Tatenhove et al., 1996). Of these moraine systems, the Ørkendalen system is perhaps the most well-dated paleo ice margin; a series of bracketing radiocarbon ages constrain the Ørkendalen system to ~6.8 cal ka BP (van Tatenhove et al., 1996). Notably, the radiocarbon-based age of the Ørkendalen Moraine was duplicated by Levy et al. (2012) and Carlson et al. (2014) who directly dated the Ørkendalen Moraine with ^{10}Be to ~6.8 and ~6.9 ka, respectively. Based on existing age constraints, deposition of the Taserqat, Sarfartôq-Avatdelq, Fjord, and Umîvît-Keglen moraines is broadly constrained to between ~11 ka to 6.8 ka, and age of the Ørkendalen Moraine is robustly constrained to 6.9–6.8 ka. We also note that a number of investigators have attempted to further refine the GrIS deglaciation chronology between the modern coast line and ice-sheet margin with ^{10}Be (Rinterknecht et al., 2009; Roberts et al., 2009; Winsor et al., 2015; Levy et al., 2018). We discuss these ^{10}Be ages in detail within the context of new ^{10}Be ages presented here in Section 6.3 during the early Holocene (Weidick, 1974; van Tatenhove et al., 1996). Shown are all individual ^{10}Be ages (ka ± 1SD analytical uncertainties) from erratic boulders perched on bedrock located beyond and between moraine systems (white boxes and black text; outliers in italics), and the arithmetic mean ± 1SD ^{10}Be age for each moraine (colored boxes and white text; Table 1; Fig. 15; Fig. 16). (B) Same as panel A, but includes all previously published ^{10}Be ages from region discussed in section 6.3 (Table S1).

4. Methods

4.1. Field methods

Bedrock in the King Harvest region, Cumberland Peninsula, primarily consists of Precambrian crystalline rocks (gneisses) of the Churchill Province (Wheeler et al., 1997; De Angelis and Kleman, 2007), whereas bedrock in the Kangerlussuaq region, southwestern Greenland, consists primarily of Archean orthogneiss (Garde and Marker, 2010). In the King Harvest region, moraine crests were mapped prior to fieldwork using aerial photographs and satellite imagery, and then checked in the field. In southwestern Greenland, we relied on the original extensive mapping of Weidick (1974) to pinpoint moraines for ^{10}Be sampling. In addition to the original mapping of Weidick (1974), we relied on aerial and satellite imagery to further characterize the surficial geology of the region. Ultimately, our moraine mapping is slightly modified from Weidick (1974); we made a pointed effort to differentiate between each moraine system versus the original mapping where moraines were undifferentiated (Fig. 3). We note that van Tatenhove et al. (1996) broadly distinguished between each moraine system and

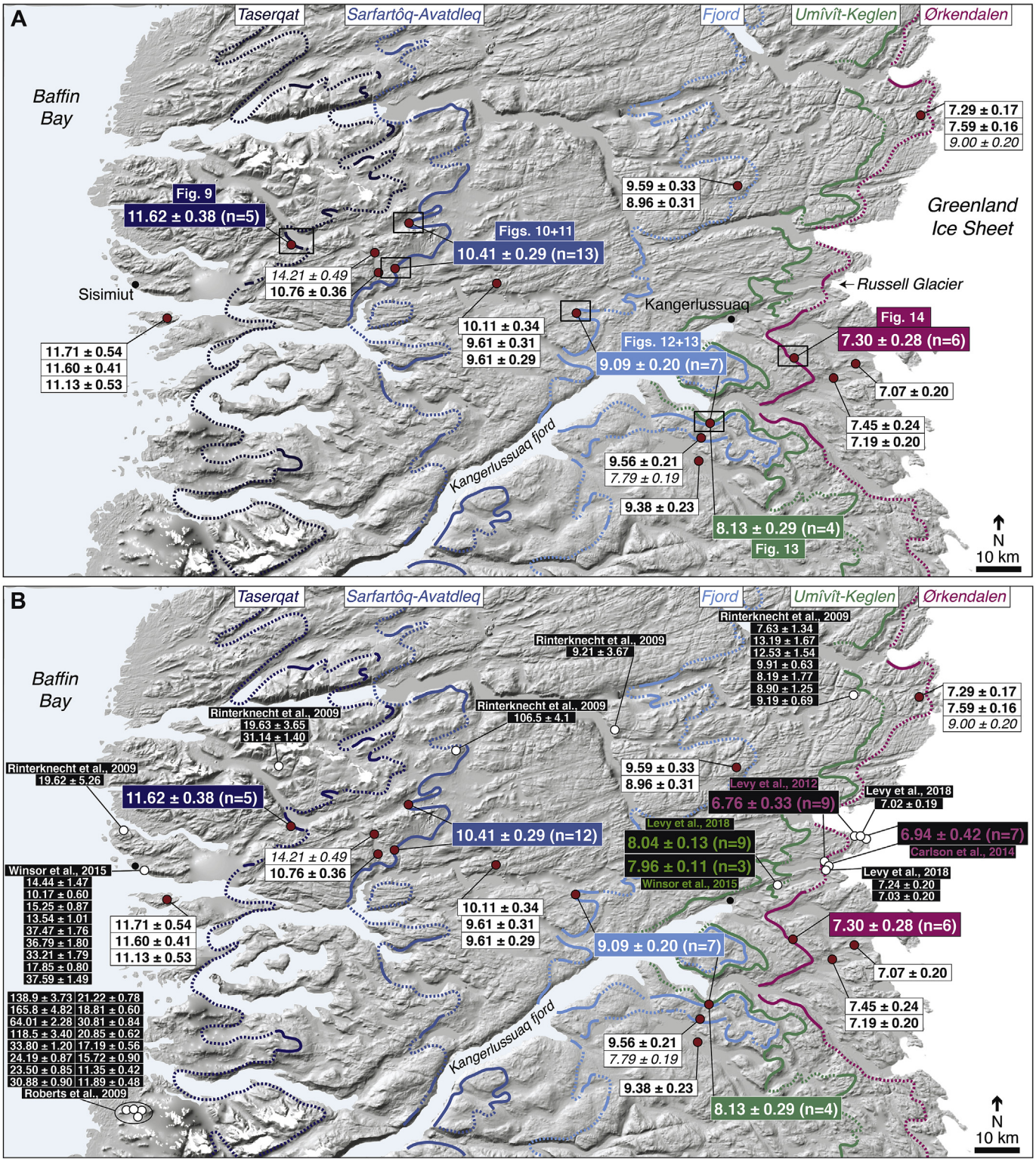

Fig. 3. (A) Moraines deposited by the GrIS between Baffin Bay and the modern ice margin during the early Holocene (Weidick, 1974; van Tatenhove et al., 1996). Shown are all individual 10Be ages (ka ± 1SD analytical uncertainties) from erratic boulders perched on bedrock located beyond and between moraine systems (white boxes and black text; outliers in italics), and the arithmetic mean ± 1SD 10Be age for each moraine (colored boxes and white text; Table 1; Fig. 15; Fig. 16). (B) Same as panel A, but includes all previously published 10Be ages from region discussed in section 6.3 (Table S1).

this differentiation further guided our mapping and sampling strategies. At every ^{10}Be sampling location (see sample locations; Fig. 3), we confirmed the original mapping of Weidick (1974), thereby increasing our confidence in the mapping accuracy in regions that have not been directly checked in the field. In Fig. 3, well-defined moraines and drift limits are marked by a solid bold line, whereas inferred limits between well-preserved moraine sections are marked with dashes. We emphasize that we only

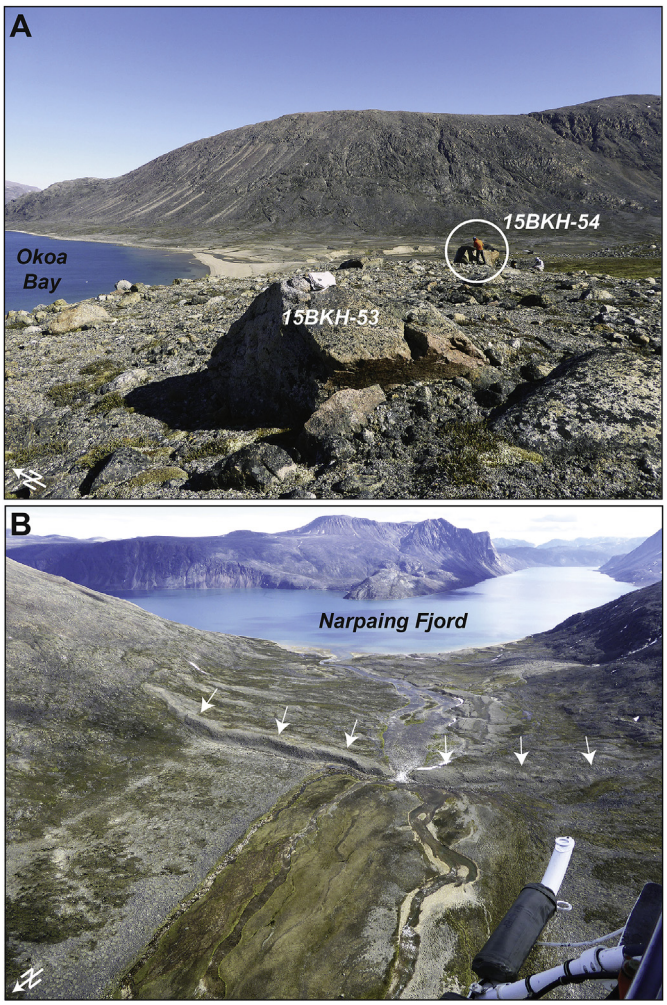

Fig. 4. (A) View to the northeast looking down the crest of the OL moraine (Fig. 2B), with representative samples 15BKH-53 (7.01 ± 0.17 ka) and 15BKH-54 (12.09 ± 0.25 ka). (B) View to the southeast looking into Narpaing Fjord (Fig. 2B) showing the NL moraine (arrows). The NL moraine was deposited by ice filling Narpaing Fjord. All ^{10}Be samples from the NL moraine were collected on the southwest side of the river channel cutting through the moraine.

targeted well-defined moraine crests or associated drift limits for moraine boulder ^{10}Be sampling.

Field work in the King Harvest moraine complex, Baffin Island, and in southwestern Greenland occurred in 2015 and 2016. In both regions ^{10}Be sampling was conducted via helicopter ground stops and by establishing several basecamps where ^{10}Be sampling was conducted over the course of several days by foot. Previous ^{10}Be sampling in southwestern Greenland has relied primarily on the field access provided by the towns of Sisimiut and Kangerlussuaq, and previous ^{10}Be ages are largely concentrated in these regions. Here, our helicopter access allowed our team to systematically visit and sample each moraine system extending from the present coastline to the ice margin (Fig. 3). Samples were collected using a Hilti brand AG500-A18 angle grinder/circular saw with diamond bit blades, and a hammer and chisel. Sample locations and elevations were collected with a handheld GPS device with a vertical uncertainty of ±5 m, and a handheld clinometer was used to measure topographic shielding by the surrounding topography. Handheld GPS units were calibrated to a known elevation each morning, typically sea level or the stated elevation of a lake derived from topographic maps. The GPS unit elevation uncertainty of ~5 m corresponds to <1% change in calculated ^{10}Be age and does not affect our interpretations or conclusions.

4.2. Geochemistry and AMS measurements

All samples from the King Harvest region (n = 61), and 53 of 62 samples from southwestern Greenland were processed at the Lamont-Doherty Earth Observatory (LDEO) cosmogenic dating laboratory (Tables 1 and 2). The remaining 9 samples from southwestern Greenland were processed at the University at Buffalo Cosmogenic Isotope Laboratory (Tables 1 and 2); in both laboratories, quartz separation and Be isolation followed well established protocols (Schaefer et al., 2009). AMS analysis for King Harvest samples was completed at the Center for Accelerator Mass Spectrometry at Lawrence Livermore National Laboratory (LLNL-CAMS; Table 1). For samples from southwestern Greenland, AMS analysis for 48 of the 62 samples was completed at the Purdue Rare Isotope Measurement (PRIME) Laboratory, and the remaining 14 samples were measured at LLNL-CAMS. In total, 75 samples were measured at LLNL-CAMS and 48 samples were measured at PRIME Lab (Tables 1 and 2). All samples, regardless of accelerator facility, were measured relative to the 07KNSTD standard with ^{10}Be/^{9}Be ratio of 2.85×10^{-12} (Nishiizumi et al., 2007). For King Harvest samples, the 1σ analytical error ranged from 1.6% to 4.3%, with an average of 2.4 ± 0.6% (Table 1). For southwestern Greenland samples, 1σ analytical error ranged from 1.7% to 3.2%, with an average of 2.5 ± 0.4% for samples measured at LLNL-CAMS (n = 14; Table 1). For samples measured at PRIME Lab, 1σ analytical error ranged from 2.8% to 5.1%, with an average of 3.5 ± 0.6% (n = 48; Table 1).

Process blank corrections for all LDEO samples were applied by taking the batch-specific blank value (expressed as # of ^{10}Be atoms) and subtracting this value from the sample ^{10}Be atom count (Table 2). For samples processed at U. Buffalo, we used a long-term lab average blank value due to building renovation that commenced in the middle of the sample dissolution (Table 2). We note that for LDEO blank BLK_2018Jan25, measured at PRIME Lab, the measured ^{10}Be/^{9}Be ratio is 0.000 ± 8.000^{-16}, which equates to 0 ± 1120 ^{10}Be atoms - effectively no detectable background ^{10}Be (Table 2). However, we use a conservative approach and apply a blank correction of 1120 ^{10}Be atoms for the 4 geologic samples this blank applies to (Table 2). Choosing to not apply a blank correction for the geologic samples processed with BLK_2018Jan25 does not, within rounding, change our reported ^{10}Be ages. Lastly, we propogate through a 1.5% uncertainty in the carrier concentration when calculating ^{10}Be concentrations

4.3. ^{10}Be age calculations

^{10}Be surface exposure ages were calculated using the Baffin Bay ^{10}Be production-rate calibration dataset (Young et al., 2013), and 'Lm' scaling (Lal, 1991; Stone, 2000) as the effects of changes in the geomagnetic field are minimal at this high latitude. The Baffin Bay production-rate calibration benefits from three independent and statistically identical calibration datasets that are combined into one calibration dataset (Briner et al., 2012; Young et al., 2013). Two of the calibration sites are from early Holocene deposits in the Jakobshavn Isbræ forefield, western Greenland, located ~200 km north of our southwestern Greenland field site (Fig. 1). The third calibration site, also from early Holocene glacial deposits, is located in north-central Baffin Island, ~300 km northwest of our King Harvest site. Ages are calculated using version 3 of the exposure age calculator found at https://hess.ess.washington.edu/, that implements an updated treatment of muon-based nuclide production (Balco et al., 2008; Balco, 2017). We do not correct nuclide concentrations for snow-cover or surface erosion; samples are almost

Table 1
Baffin Island and southwestern Greenland ^{10}Be sample information.

Sample	Latitude	Longitude	Elevation (m asl)	Thickness (cm)	Shielding	Quartz (g)	Carrier added (g)[a]	^{10}Be/^{9}Be ratio (10^{-14})[b]	±1σ Uncertainty (10^{-15})	Blank-corrected ^{10}Be concentration (atoms g^{-1})[c]	Blank-corrected ^{10}Be conc. uncertainty (atoms g^{-1})[c]	Age ka (Lm)	Age ka uncertainty	AMS Facility
Baffin Island - King Harvest														
Valley floor moraine (VF)														
15BKH-01	67.8315	−65.7186	99	2.43	0.995	15.0398	0.1809	13.8366	2.2284	116,090	1879	*25.48*	*0.42*	LLNL-CAMS
15BKH-02	67.8313	−65.7189	109	1.47	0.995	15.0246	0.1803	8.1541	1.4053	68,095	1185	*14.62*	*0.26*	LLNL-CAMS
15BKH-03	67.8301	−65.7196	113	1.10	0.995	16.2948	0.1809	7.2399	1.4709	55,089	1132	11.73	0.24	LLNL-CAMS
15BKH-05	67.8297	−65.7198	128	1.04	0.995	16.8382	0.1820	7.6984	1.5618	57,056	1169	11.94	0.25	LLNL-CAMS
15BKH-06	67.8299	−65.7209	128	2.39	0.995	13.0090	0.1817	5.8347	1.3597	56,587	1335	11.98	0.28	LLNL-CAMS
15BKH-07	67.8291	−65.7196	130	1.45	0.995	20.7932	0.1831	15.8212	2.6479	95,966	1624	*20.16*	*0.34*	LLNL-CAMS
15BKH-09	67.8291	−65.7196	129	1.97	0.996	20.0691	0.1832	15.0257	2.8181	94,463	1790	*19.99*	*0.38*	LLNL-CAMS
15BKH-11	67.8271	−65.7210	147	1.48	0.995	21.9316	0.1802	9.9174	1.8511	56,764	1067	11.68	0.22	LLNL-CAMS
15BKH-12	67.8246	−65.6950	137	3.46	0.998	21.6251	0.1813	9.4130	1.7567	54,961	1033	11.58	0.22	LLNL-CAMS
15BKH-13	67.8245	−65.6958	137	2.19	0.998	22.3214	0.1806	17.4460	3.3621	98,531	1905	*20.60*	*0.40*	LLNL-CAMS
15BKH-14	67.8244	−65.6967	137	3.69	0.998	22.1298	0.1797	9.8568	1.8123	55,754	1032	11.77	0.22	LLNL-CAMS
15BKH-15	67.8242	−65.6973	136	2.57	0.998	9.3870	0.1800	4.1873	1.7858	56,022	2402	11.73	0.51	LLNL-CAMS
15BKH-16	67.8242	−65.6974	136	1.70	0.998	18.0574	0.1834	8.0005	1.9790	55,782	1408	11.60	0.29	LLNL-CAMS
												Mean ± 1 S.D.	**11.75 ± 0.14 (0.25)**	
Okoa lateral moraine (OL)														
15BKH-48	67.8549	−65.7955	80	2.01	0.987	14.1485	0.1833	9.3874	2.2113	85,040	2011	*19.12*	*0.45*	LLNL-CAMS
15BKH-49	67.8553	−65.7943	83	2.93	0.987	21.6057	0.1831	8.9437	1.8947	52,991	1128	11.94	0.26	LLNL-CAMS
15BKH-50	67.8555	−65.7934	81	2.12	0.987	14.5216	0.1828	9.2396	1.7319	81,324	1532	*18.28*	*0.35*	LLNL-CAMS
15BKH-51	67.8560	−65.7921	73	3.06	0.987	17.2412	0.1831	6.9084	1.2697	49,866	961	11.38	0.22	LLNL-CAMS
15BKH-52	67.8561	−65.7916	72	2.25	0.987	18.8722	0.1830	7.6720	1.9568	51,986	1332	11.80	0.30	LLNL-CAMS
15BKH-53	67.8563	−65.7909	72	2.29	0.988	20.2922	0.1829	5.0748	1.1540	30,920	746	*7.01*	*0.17*	LLNL-CAMS
15BKH-54	67.8564	−65.7903	72	2.01	0.987	17.6822	0.1822	7.4130	1.5302	53,370	1108	12.09	0.25	LLNL-CAMS
												Mean ± 1 S.D.	**11.79 ± 0.32 (0.38)**	
Narpaing lateral moraine (NL)														
15BKH-41	67.7925	−65.6566	60	2.02	0.997	17.0393	0.1816	6.2000	1.3988	46,173	1046	10.50	0.24	LLNL-CAMS
15BKH-42	67.7927	−65.6564	57	2.66	0.997	25.0576	0.1822	8.9864	2.2444	44,562	1138	10.22	0.26	LLNL-CAMS
15BKH-43	67.7927	−65.6565	57	2.38	0.997	12.5808	0.1819	4.4957	1.0183	45,311	1038	10.37	0.24	LLNL-CAMS

15BKH-44	67.7928	−65.6565	56	1.62	0.997	16.3627	0.1824	5.8366	1.2959	45,416	1016	10.34	0.23	LLNL-CAMS
15BKH-45	67.7928	−65.6564	57	1.66	0.997	15.5530	0.1827	5.5386	1.1525	45,405	953	10.33	0.22	LLNL-CAMS
15BKH-46	67.7932	−65.6563	52	2.51	0.997	20.0616	0.1826	7.1561	1.7798	44,292	1137	10.21	0.26	LLNL-CAMS
15BKH-47	67.7934	−65.6562	49	2.33	0.997	19.8621	0.1850	7.0222	1.3250	45,693	868	10.55	0.20	LLNL-CAMS
												Mean ± 1 S.D.	**10.36 ± 0.13 (0.23)**	
Narpaing - upfjord														
15BKH-55	67.6704	−65.3733	78	2.03	0.987	22.8309	0.1811	7.5538	2.6819	40,638	1481	9.14	0.33	LLNL-CAMS
15BKH-56	67.6705	−65.3734	76	1.08	0.997	16.6343	0.1815	5.4840	1.0987	41,755	844	9.25	0.19	LLNL-CAMS
15BKH-57	67.6710	−65.3736	73	2.40	0.987	25.1999	0.1818	8.0884	2.8771	39,637	1444	8.99	0.33	LLNL-CAMS
15BKH-58	67.6723	−65.3742	64	1.69	0.987	25.9043	0.1813	8.6622	1.6433	41,235	806	9.40	0.18	LLNL-CAMS
15BKH-59	67.6734	−65.3742	59	1.57	0.987	20.8735	0.1820	7.0261	2.6571	41,484	1613	9.50	0.37	LLNL-CAMS
15BKH-60	67.6743	−65.3743	60	1.80	0.987	20.5337	0.1823	7.8112	2.6454	47,074	1635	*10.79*	*0.37*	LLNL-CAMS
15BKH-61	67.6736	−65.3742	58	2.10	0.987	19.6892	0.1822	7.1971	2.0563	45,126	1328	*10.39*	*0.30*	LLNL-CAMS
												Mean ± 1 S.D.	**9.26 ± 0.20 (0.26)**	
King Harvest 1 (K1)														
15BKH-35	67.8024	−65.7387	388	1.22	0.996	10.7828	0.1820	6.5357	1.4669	75,560	1716	12.02	0.27	LLNL-CAMS
15BKH-36	67.8023	−65.7357	386	1.95	0.996	17.5461	0.1807	10.0714	1.9748	72,560	1426	11.64	0.23	LLNL-CAMS
15BKH-37	67.8023	−65.7342	375	1.03	0.996	11.5802	0.1815	6.8209	1.4998	73,245	1629	11.79	0.26	LLNL-CAMS
15BKH-38	67.8022	−65.7335	370	2.13	0.996	17.4681	0.1825	15.7394	5.1388	115,116	3763	*18.82*	*0.62*	LLNL-CAMS
15BKH-39	67.8019	−65.7300	350	1.14	0.996	10.9993	0.1817	6.3153	1.4156	71,437	1621	11.81	0.27	LLNL-CAMS
15BKH-40	67.8020	−65.7306	357	1.06	0.996	11.4736	0.1814	6.7446	1.4247	72,422	1548	11.88	0.25	LLNL-CAMS
												Mean ± 1 S.D.	**11.83 ± 0.14 (0.25)**	
King Harvest 2 (K2)														
15BKH-17	67.8181	−65.6932	129	1.68	0.998	15.9182	0.1800	6.0113	1.4122	47,492	1120	9.95	0.24	LLNL-CAMS
15BKH-18	67.8177	−65.6916	129	2.04	0.998	16.8762	0.1792	6.6396	2.3738	49,273	1767	10.35	0.37	LLNL-CAMS
15BKH-19	67.8141	−65.6820	103	1.49	0.998	18.6035	0.1802	18.8897	5.4888	128,114	3727	*27.71*	*0.81*	LLNL-CAMS
15BKH-20	67.8139	−65.6887	121	1.25	0.998	16.6977	0.1805	6.6897	1.5131	50,541	1147	10.65	0.24	LLNL-CAMS
15BKH-26	67.8034	−65.7371	381	3.83	0.990	22.4915	0.1829	11.0636	1.9143	61,492	1090	10.12	0.18	LLNL-CAMS
15BKH-28	67.8051	−65.7191	290	1.98	0.991	20.0545	0.1831	17.3294	3.7369	108,097	2354	*19.27*	*0.42*	LLNL-CAMS
15BKH-63	67.8186	−65.7055	158	2.82	0.996	10.0295	0.1830	4.0832	1.7245	50,113	2210	10.28	0.45	LLNL-CAMS
												Mean ± 1 S.D.	**10.27 ± 0.26 (0.32)**	

(*continued on next page*)

Table 1 (*continued*)

Sample	Latitude	Longitude	Elevation (m asl)	Thickness (cm)	Shielding	Quartz (g)	Carrier added (g)[a]	$^{10}Be/^{9}Be$ ratio (10^{-14})[b]	±1σ Uncertainty (10^{-15})	Blank-corrected ^{10}Be concentration (atoms g^{-1})[c]	Blank-corrected ^{10}Be conc. uncertainty (atoms g^{-1})[c]	Age ka (Lm)	Age ka uncertainty	AMS Facility
King Harvest 3 (K3)														
15BKH-23	67.8033	−65.7418	390	1.46	0.991	19.0815	0.1830	8.4154	2.7242	55,422	1819	8.85	0.29	LLNL-CAMS
15BKH-24	67.8033	−65.7416	388	1.95	0.991	19.3372	0.1835	8.5343	1.9665	55,620	1307	8.94	0.21	LLNL-CAMS
15BKH-25	67.8035	−65.7384	387	2.65	0.990	30.1124	0.1827	13.6118	2.5505	56,855	1078	9.21	0.17	LLNL-CAMS
15BKH-27	67.8048	−65.7287	342	2.89	0.993	26.1169	0.1822	11.6958	1.9363	55,794	945	9.46	0.16	LLNL-CAMS
15BKH-62	67.8148	−65.7268	271	2.18	0.996	15.9068	0.1821	6.5398	1.2509	52,285	1008	9.45	0.18	LLNL-CAMS
15BKH-64	67.8173	−65.7050	176	2.38	0.996	19.1583	0.1825	3.7021	1.0240	23,656	707	*4.74*	*0.14*	LLNL-CAMS
15BKH-65	67.8128	−65.6989	145	3.08	0.996	22.0508	0.1820	7.8374	1.5188	45,206	881	9.43	0.18	LLNL-CAMS
15BKH-66	67.8128	−65.6994	155	2.86	0.996	17.0792	0.1822	2.1394	4.0105	159,837	3001	*33.10*	*0.63*	LLNL-CAMS
15BKH-67	67.8080	−65.7013	165	2.35	0.998	15.9246	0.1823	5.6932	1.2101	45,488	975	9.21	0.20	LLNL-CAMS
15BKH-68	67.8073	−65.7057	195	2.02	0.998	22.8305	0.1829	10.8603	2.1774	59,456	1217	*11.62*	*0.24*	LLNL-CAMS
												Mean ± 1 S.D.	**9.21 ± 0.25 (0.30)**	
King Harvest upvalley														
15BKH-30	67.8045	−65.7662	446	1.03	0.997	17.9824	0.1804	8.8784	2.4872	62,294	1749	9.32	0.26	LLNL-CAMS
15BKH-31	67.8050	−65.7653	442	1.76	0.997	14.5829	0.1806	6.7962	1.3734	58,827	1193	8.89	0.18	LLNL-CAMS
15BKH-32	67.8047	−65.7647	433	1.45	0.997	17.6963	0.1806	8.3538	1.6712	59,619	1196	9.07	0.18	LLNL-CAMS
15BKH-34	67.8079	−65.7413	310	1.68	0.996	17.1176	0.1802	7.1913	1.8080	52,920	1335	9.15	0.23	LLNL-CAMS
												Mean ± 1 S.D.	**9.11 ± 0.18 (0.24)**	
Southwestern Greenland														
Erratic boulders														
16GRO-01	67.4089	−49.8130	565	3.25	1	32.9555	0.6021	1.1907	2.6957	54,149	1226	7.29	0.17	LLNL-CAMS
16GRO-02	67.4085	−49.8291	581	3.00	1	32.4943	0.6074	1.4623	3.1490	68,040	1465	*9.00*	*0.20*	LLNL-CAMS
16GRO-03	67.4184	−49.7963	575	1.00	1	41.0266	0.6054	1.5781	3.3134	57,962	1217	7.59	0.16	LLNL-CAMS
16GRO-04	66.9126	−50.1802	172	2.50	1	35.2685	0.6078	0.8827	2.7836	37,865	1194	7.45	0.24	LLNL-CAMS
16GRO-06	66.9119	−50.1678	230	2.00	1	34.9986	0.6075	0.9025	2.5378	38,991	1096	7.19	0.20	LLNL-CAMS
16GRO-07	66.9423	−50.0955	273	1.50	1	30.2588	0.6065	0.8058	2.3485	40,202	1172	7.07	0.20	LLNL-CAMS
16GRO-09	66.7591	−50.7890	447	2.00	1	32.7152	0.6139	1.3770	3.0112	64,318	1406	9.56	0.21	LLNL-CAMS
16GRO-11	66.7665	−50.8143	315	2.50	1	35.1616	0.6181	1.0486	2.5603	45,884	1120	*7.79*	*0.19*	LLNL-CAMS
16GRO-26	66.7302	−50.8119	308	2.00	1	32.7920	0.6241	1.1628	2.7987	55,086	1326	9.38	0.23	LLNL-CAMS
	66.8706	−53.4602	234	1.25	1	15.5896	0.1829	0.7967	3.6639	64,169	2972	11.71	0.54	PRIME

16GRO-41														
16GRO-42	66.8721	−53.4592	239	1.22	1	11.6444	0.1815	0.5771	2.6725	61,328	2922	11.13	0.53	PRIME
16GRO-44	66.8737	−53.4556	230	2.31	1	18.1350	0.1820	0.9144	3.1638	62,793	2215	11.60	0.41	PRIME
16GRO-46	67.0558	−52.5139	302	2.20	0.996	23.8858	0.1816	1.5798	5.3957	82,400	2837	*14.21*	*0.49*	PRIME
16GRO-57	67.0313	−52.4662	333	2.40	0.998	30.0362	0.1833	1.5345	5.0943	64,437	2146	10.76	0.36	PRIME
16GRO-67	67.0262	−51.8950	510	1.33	1	31.1948	0.1834	1.7068	5.0629	69,065	2056	9.61	0.29	PRIME
16GRO-68	67.0233	−51.8981	516	2.48	1	30.0651	0.1829	1.6435	5.2086	68,808	2190	9.61	0.31	PRIME
16GRO-69	67.0234	−51.8966	516	2.21	1	28.6967	0.1833	1.6496	5.5469	72,516	2449	10.11	0.34	PRIME
16GRO-76	67.2584	−50.7309	769	1.47	1	11.6904	0.1836	0.8128	2.7589	87,284	3004	9.59	0.33	PRIME
16GRO-78	67.2592	−50.7329	773	1.16	1	30.0159	0.1832	1.9546	6.7152	82,132	2832	8.96	0.31	PRIME
Taserqat Moraine														
16GRO-32	67.0493	−52.9097	400	2.34	1	27.5000	0.1817	1.6531	5.5253	77,771	2620	12.13	0.41	PRIME
16GRO-33	67.0484	−52.9093	417	3.22	1	20.4639	0.1813	1.1892	4.4758	72,190	2749	11.15	0.43	PRIME
16GRO-34	67.0499	−52.9119	404	2.63	1	22.2613	0.1815	1.3217	4.4228	73,877	2500	11.50	0.39	PRIME
16GRO-35	67.0512	−52.9148	397	1.69	1	22.7147	0.1812	1.3483	3.7197	73,744	2063	11.47	0.32	PRIME
16GRO-36	67.0533	−52.9175	384	1.84	1	23.0832	0.1814	1.3935	3.7142	75,090	2029	11.85	0.32	PRIME
16GRO-37	67.0525	−52.9171	393	1.97	1	26.7593	0.1818	3.1659	6.1798	147,822	2901	*23.20*	*0.46*	PRIME
												Mean ± 1 S.D.	**11.62 ± 0.38 (0.43)**	
Sarfartôq-Avatdleq Moraine														
16GRO-49	67.0303	−52.3956	303	3.59	1	22.7056	0.1810	1.0781	3.7803	58,863	2094	10.20	0.36	PRIME
16GRO-51	67.0301	−52.3936	299	2.49	1	26.1454	0.1816	1.2327	4.9590	58,682	2384	10.12	0.41	PRIME
16GRO-52	67.0318	−52.3943	315	1.89	1	21.6163	0.1811	1.0390	4.6230	59,607	2684	10.07	0.46	PRIME
16GRO-54	67.0344	−52.3899	313	2.42	1	20.1321	0.1821	0.9937	2.7018	60,687	1685	10.32	0.29	LLNL-CAMS
16GRO-55	67.0384	−52.3779	366	2.33	1	20.9769	0.1810	1.0795	3.0059	62,971	1786	10.15	0.29	LLNL-CAMS
16GRO-56	67.0333	−52.3923	299	1.77	1	20.9231	0.1833	1.0218	1.7539	60,478	1065	10.37	0.18	LLNL-CAMS
16GRO-59	67.1269	−52.3463	636	1.12	0.994	11.0795	0.1824	0.7401	1.6741	83,544	1914	10.37	0.24	LLNL-CAMS
16GRO-60	67.1256	−52.3404	639	1.80	0.995	23.0070	0.1822	1.6581	4.8294	89,983	2640	11.19	0.33	PRIME
16GRO-61	67.1256	−52.3402	637	1.54	0.995	11.2967	0.1824	0.7578	2.7030	83,396	3030	10.37	0.38	PRIME
16GRO-62	67.1265	−52.3478	627	1.40	0.994	9.7126	0.1832	0.6545	1.6268	84,578	2132	10.61	0.27	LLNL-CAMS
16GRO-63	67.1245	−52.3486	616	1.25	0.995	30.1541	0.1833	2.0067	6.5484	83,985	2749	10.62	0.35	PRIME
	67.1250	−52.3425	624	3.04	0.995	14.8697	0.1823	0.9828	3.5608	82,311	3020	10.48	0.39	PRIME

(*continued on next page*)

Table 1 (*continued*)

Sample	Latitude	Longitude	Elevation (m asl)	Thickness (cm)	Shielding	Quartz (g)	Carrier added (g)[a]	$^{10}Be/^{9}Be$ ratio (10^{-14})[b]	±1σ Uncertainty (10^{-15})	Blank-corrected ^{10}Be concentration (atoms g^{-1})[c]	Blank-corrected ^{10}Be conc. uncertainty (atoms g^{-1})[c]	Age ka (Lm)	Age ka uncertainty	AMS Facility
16GRO-64														
16GRO-65	67.1266	−52.3325	630	1.84	0.995	27.9849	0.1821	1.8765	5.3561	83,721	2404	10.50	0.30	PRIME
16GRO-66	67.1266	−52.3325	629	1.07	0.995	30.1746	0.1834	2.2326	7.9210	93,445	3323	*11.66*	*0.42*	PRIME
												Mean ± 1 S.D.	**10.41 ± 0.29 (0.35)**	
Fjord Moraine														
16GRO-12	66.7974	−50.7798	354	2.34	1	35.3518	0.2020	1.3782	3.3780	54,349	1334	8.87	0.22	PRIME
16GRO-13	66.7996	−50.7722	376	2.28	0.998	32.3242	0.1830	2.4188	6.5040	93,977	2539	*15.06*	*0.41*	PRIME
16GRO-14	66.7996	−50.7719	376	2.12	0.998	32.6750	0.1827	1.5063	4.3618	57,692	1684	9.22	0.27	PRIME
16GRO-15	66.7999	−50.7703	380	0.90	0.996	32.2519	0.1827	1.5053	5.2453	58,411	2050	9.23	0.33	PRIME
16GRO-16	66.7998	−50.7712	381	2.49	0.998	18.4242	0.1821	0.8220	3.4052	55,417	2329	8.84	0.37	PRIME
16GRO-71	66.9894	−51.4716	243	1.50	1	25.5744	0.1818	1.2757	4.3422	62,062	2132	*11.25*	*0.39*	PRIME
16GRO-73	66.9901	−51.4672	224	1.33	1	29.4850	0.1818	1.2052	4.7100	50,837	2005	9.38	0.37	PRIME
16GRO-74	66.9893	−51.4645	223	2.30	1	30.3036	0.1834	1.1616	4.2667	48,198	1785	8.97	0.33	PRIME
16GRO-75	66.9894	−51.4633	220	3.67	1	27.2409	0.1840	1.0430	3.0354	48,267	1420	9.11	0.27	PRIME
												Mean ± 1 S.D. 9.09 ± 0.20 (0.26)		
Recessional crest														
16GRO-22	66.8016	−50.7576	367	1.98	0.998	35.0453	0.2030	1.3131	3.6847	52,492	1472	8.45	0.24	PRIME
16GRO-23	66.8020	−50.7557	370	2.47	0.995	35.0640	0.2023	1.3440	6.2247	53,514	2478	8.65	0.40	PRIME
16GRO-24	66.8020	−50.7549	370	1.74	0.996	35.3993	0.2030	1.3889	4.2199	54,969	1671	8.82	0.27	PRIME
												Mean ± 1 S.D.	**8.64 ± 0.19 (0.25)**	
Umîvît-Keglen Moraine														
16GRO-17	66.8060	−50.7630	313	1.83	1	25.3022	0.1826	1.0222	4.2850	83,354	3532	*14.13*	*0.60*	PRIME
16GRO-18	66.8058	−50.7629	312	0.80	1	35.2285	0.1822	1.3311	4.6530	47,126	1662	7.92	0.28	PRIME
16GRO-19	66.8058	−50.7617	313	1.53	0.999	33.9045	0.1819	1.3020	5.1019	50,492	1995	8.54	0.34	PRIME
16GRO-20	66.8058	−50.7613	314	2.30	0.999	30.3979	0.1826	1.1369	3.5082	46,812	1458	7.95	0.25	PRIME
16GRO-21	66.8061	−50.7603	314	3.03	0.999	30.2733	0.1832	1.1410	4.2782	47,334	1790	8.09	0.31	PRIME
												Mean ± 1 S.D.	**8.13 ± 0.29 (0.32)**	
Ørkendalen Moraine complex														
16GRO-85	66.9439	−50.3956	404	1.01	1	10.5969	0.1836	0.4106	2.0555	48,225	2479	7.42	0.38	PRIME
	66.9461	−50.4028	402	2.23	1	30.9805	0.1861	1.2038	3.7442	49,573	1555	7.72	0.24	PRIME

16GRO-86												
16GRO-87	66.9454	−50.4079	429	1.75	1	30.1641	0.1800	1.1095	3.8117	45,372	1573	6.85	0.24	PRIME
16GRO-88	66.9452	−50.4084	435	2.19	1	30.2594	0.1830	1.1694	4.5658	48,485	1908	7.31	0.29	PRIME
16GRO-89	66.9450	−50.4110	454	1.95	1	29.7947	0.1834	1.1676	3.4987	49,276	1490	7.28	0.22	PRIME
16GRO-90	66.9448	−50.4113	456	2.47	1	30.0518	0.1831	1.1699	3.7993	48,868	1601	7.23	0.24	PRIME
												Mean ± 1 S.D.	**7.30 ± 0.28 (0.31)**	

Ages are calculated using version 3 of the exposure age calculator found at https://hess.ess.washington.edu/(wrapper: 3.0, muons: 1A, consts: 3.0.3), which implements an updated treatment of muon-based production (Balco et al., 2008; Balco, 2017). All ages are calcualted using 'Lm' scaling and a Baffin Bay production rate of 4.04 ± 0.07 atoms g^{-1} yr^{-1} (Young et al., 2013). This value has been updated from the CRONUS v2 value of 3.96 ± 0.07 atoms g^{-1} yr^{-1}; the calibration dataset is the same. All samples use a density of 2.65 g cm^{-3}, standard air pressure 'std', and an effective attenuation length of 160 g cm^{-2}. ^{10}Be concentrations are reported relative to 07KNSTD with a reported ratio of 2.85 × 10^{-12} using a ^{10}Be half-life of 1.36 × 10^{6} years (Nishiizumi et al., 2007).

Numbers in parentheses are the moraine age uncertainties that include the uncertainty in the ^{10}Be production rate calibration dataset. Moraine ages with the production rate uncertainty must be used when comparing the Baffin Bay moraines to any independent record that is not on the Baffin Bay-Arctic ^{10}Be timescale.

[a] Samples were spiked with LDEO carriers 5.1 and 6 with evaporation-corrected ^{9}Be concentrations ranging from 1028 to 1049 ppm, and a Buffalo carrier with concentrations ranging from 372.5 to 1049 ppm (see Table 2).

[b] Samples were measured at either the Lawrence Livermore National Laboratory - Center for Accelerator Mass Spectrometry (LLNL-CAMS) or the Purdue Rare Isotope Measurement Laboratory (PRIME). Ratios are not corrected for ^{10}Be detected in procedural blanks.

[c] Concentrations are blank corrected by subtracting the total number of ^{10}Be atoms in the process blank (Table 2); see Table 2 for process blank values and description of the Buffalo blank correction.

exclusively from windswept locations and many surfaces still retained primary glacial features. Individual ^{10}Be ages are presented and discussed with 1-sigma analytical uncertainties, and moraine ages exclude the ^{10}Be production-rate uncertainty when we are comparing moraine ages within Baffin Bay. When moraine ages are compared to independent records of climate variability or ice-sheet change, the production rate uncertainty is propagated through in quadrature (Tables 1 and S1).

4.3.1. The effects of isostatic rebound on ^{10}Be production and ^{10}Be age calculations

We do not correct ^{10}Be ages for the effects of isostatic rebound. All of our sample locations have experienced varying degrees of isostatic uplift since the timing of local deglaciation and therefore our sample sites have rested at an elevation that is lower than their current elevation for a portion of their total exposure histories. Because the rate of ^{10}Be production is lower at lower elevations (i.e. more overriding atmosphere), correcting our ^{10}Be ages solely for the effects of isostatic uplift by using a time-averaged sample elevation, would result in older ^{10}Be ages. However, the relatively straightforward effects of elevation change driven by isostatic rebound on ^{10}Be production are counteracted to some degree by atmospheric pressure changes in ice-marginal settings not related to sample elevation change (Staiger et al., 2007). In addition to a sample site moving up or down in the atmosphere through isostatic uplift or depression, atmospheric compression and pressure anomalies in ice-margin environments influences ^{10}Be production and acts to offset elevation-related changes in ^{10}Be production (Staiger et al., 2007). Whereas the effects of isostatic uplift, assuming a stationary atmosphere, on ^{10}Be production may be relatively straightforward to quantify, this correction only results in a maximum ^{10}Be age and is counteracted by harder-to-quantify atmospheric pressure changes unrelated to sample-site elevation change.

The unique relationship between our sample locations and the Baffin Bay ^{10}Be production-rate calibration sites may also indicate that any elevation- or atmospheric pressure-based correction on ^{10}Be production may not be required. The Baffin Bay ^{10}Be production-rate calibration dataset spans the last ~9.2 ka and comprises ice-marginal sites that have undergone ~45–60 m of isostatic uplift since local deglaciation (Long et al., 2006; Briner et al., 2007; Young et al., 2013a). Both the ^{10}Be calibration dataset exposure duration and amount of uplift are similar to the exposure and uplift histories of the unknown-age sample sites considered here, with the exception of our westernmost samples in southwestern Greenland that may have undergone up to 120 m of uplift (Funder and Hansen, 1996). Any errors in the calculated ^{10}Be age presented here that are introduced by not correcting for isostatic uplift or non-uplift related atmospheric pressure changes are effectively offset by these same corrections not being made in the ^{10}Be production-rate calibration datasets that share similar exposure and uplift histories with our new sample sites. Making neither a correction for isostatic uplift or atmospheric pressure anomalies likely results in a^{10}Be age that has less uncertainty than making a correction for one of these variables while ignoring the other.

4.3.2. Re-calculating previously published ^{10}Be ages

Previously published ^{10}Be ages listed in Table S1 have been recalculated using the aforementioned methods to make these ages directly comparable to our new ^{10}Be ages presented here. We have calculated and plotted ^{10}Be ages from the Marrait Moraine, located in the Jakobshavn Isbræ forefield, using the Baffin Bay ^{10}Be production-rate calibration dataset (Young et al., 2011, Young et al., 2013a). However, ^{10}Be concentrations from moraine boulders on the Marrait Moraine serve as one of the calibration datasets within

Table 2
Process blank ^{10}Be data.

Sample ID	Carrier added (g)	Carrier concentration[a]	^{10}Be/^{9}Be ratio ± 1σ (10^{-16})	^{10}Be atoms	Samples applied to (Table 1):
LDEO Carrier 5.1					
BLK1_2016Feb10	0.1811	1047.06	4.623 ± 1.248	*5859 ± 1582*	15BKH-01, -02, −06, −11, −12, −13, −14
BLK_2016Mar18	0.1815	1048.56	1.881 ± 0.641	*2393 ± 816*	15BKH-15, -17, −18, −19, −20, −30, −31, −32, −34, −36, −38, −41
BLK_2016May13	0.1812	1049.02	2.648 ± 1.052	*3364 ± 1336*	15BKH-43, -44, −45, −47, −48, −49, −50, −52, −54, −56, −62, −65, −66, −67
LDEO Carrier 6					
BLK1_2016Sep19	0.1831	1034.12	5.509 ± 3.243	*6973 ± 4105*	15BKH-07, -09, −16, −23, −24, −25
BLK_2016Oct27	0.1829	1032.04	10.194 ± 3.291	*12,863 ± 4153*	15BKH-26, -27, −28, −42, −46, −51, −53, −63, −64, −68
BLK_2017Jan21	0.1812	1029.00	5.626 ± 5.222	*7011 ± 6508*	16GRO-32, -33, −34, −35, −36, −37, −42, −44, −46, −49, −51, −52
BLK_2017Mar03	0.1816	1037.16	16.635 ± 2.456	*20,588 ± 3093*	15BKH-55, -57, −58, −59, −60, −61; 16GRO-54, -55, −56
BLK_2017May12	0.1814	1029.85	7.483 ± 3.539	*9344 ± 4419*	16GRO-13, -14, −15, −16, −17, −18, −19, −60, −61, −64, −65, −71, −73
BLK_2017Sep18	0.1839	1031.63	7.121 ± 2.794	*9035 ± 3543*	16GRO-20, -21, −74, −75, −76, −85, −86, −87, −88, −89, −90
BLK1_2017Nov6	0.1838	1031.98	3.778 ± 2.967	*4790 ± 3762*	16GRO-41, -57, −63, −66, −67, −68, −69, −78
BLK2_2017Nov6	0.1826	1031.98	4.452 ± 1.949	*5607 ± 2455*	16GRO-59, -62
BLK_2017Nov10	0.1825	1032.05	4.631 ± 1.399	*5831 ± 1762*	15BKH-03, -05, −35, −37, −39, −40
BLK_2018Jan25	0.2027	1033.10	0.000 ± 8.000	*0 ± 1120*	16GRO-12, -22, −23, −24
Buffalo[a]					
BLK_2017June16	0.5936	372.5	20.00 ± 15.13	*29,560 ± 10,346*	16GRO-01, 02, 03, 04, 06, 07, 09, 11, −26

All ^{10}Be concentrations are reported relative to 07KNSTD with a reported ratio of 2.85×10^{-12} using a ^{10}Be half-life of 1.36×10^{6} years (Nishiizumi et al., 2007).
We conservatively calculate a value of 1120 atoms in BLK_2018Jan25 using the reported uncertainty in the reported ratio.
[a] Buffalo samples are corrected using a long-term blank value. The stated ratio is the long-term lab average used to calculate the number of ^{10}Be atoms.

the Baffin Bay ^{10}Be production-rate calibration. The Marrait Moraine is independently dated by radiocarbon to 9175 ± 45 cal yr BP (Young et al., 2013b, 2013a), and when converting measured ^{10}Be concentrations in Marrait Moraine boulders to ^{10}Be age using the Baffin Bay production rate, the moraine age is 9.21 ± 0.10 ka (n = 6). Of course, this is circular logic − using a production-rate calibration based partially on "tuning" the calibration dataset to 9175 ± 45 cal yr BP to then calculate a ^{10}Be age of 9.21 ± 0.10 ka. However, calculating ^{10}Be ages for Marrait Moraine boulders using the independent and statistically identical northeastern North America ^{10}Be production-rate calibration dataset (Balco et al., 2009) results in ^{10}Be ages that are 1.3% older, and does not affect our interpretation of the Marrait Moraine age discussed below; the same can be said if using the statistically identical high-latitude Rannoch Moor ^{10}Be production-rate calibration dataset (Putnam et al., 2019).

4.4. Age model of carbonate record from MD99-2236 and time series analysis

We developed a modified age model for sediment core MD99-2236 from the Cartwright Saddle using Bacon v. 2.2 (Blaauw and Christen, 2011) based on all 24 radiocarbon ages as published in Jennings et al. (2015). We included an additional age at 11,550 ± 100 cal yr BP based on correlation of the initial %$CaCO_3$ increase at 1795.5 cm depth with the well-dated record from Pearce et al. (2015). All radiocarbon ages were calibrated as originally reported in Jennings et al. (2015) using a marine reservoir age of 450 years (ΔR = 50 ± 50 years) and the Marine13 calibration curve (Reimer et al., 2013). For the model, section thickness was set at 1 cm and mean accumulation rate for the prior was 5 mm/yr. We used the default student-t distributions ($t_a = 3$, $t_b = 4$) for all age points except at 1795.5 cm, the tie point with Pearce et al. (2015) which we set to low uncertainty ($t_a = 30$, $t_b = 31$) and ages at 1071, 1638, 1768, 1797, and 1823 cm depth, which we set to high uncertainty ($t_a = 0$, $t_b = 1$) because these ages were excluded by Jennings et al. (2015) or disagreed with the well-dated tie point at 1795.5 cm (Pearce et al., 2015).

We incorporated age-model uncertainty into the MD99-2236 detrital carbonate and Sikuiui Lake summer temperature records we present here. To do so, we placed all proxy and chronology data in Lipd files (McKay and Emile-Geay, 2016), and analyzed the data in the software package GeoChronR (McKay et al., 2018). We then plotted each record with the median of the age ensemble and the 1 and 2 sigma uncertainty. Our age-model for MD99-2236 results in peaks of carbonate weight percentage that differ slightly in age than as originally reported by Jennings et al. (2015). Most notably, Jennings et al. (2015) reported an age of 8.15 ka BP for DCP-7, whereas here, DCP-7 falls at 7.95 ka BP. Despite the slight age offset, we agree with the original interpretation of Jennings et al. (2015) that links DCP7 to the 8.2 ka event as expressed in Greenland ice cores.

5. Results

5.1. King Harvest geomorphology

We mapped the King Harvest moraine complex and assigned each moraine to the body of ice that it was deposited by: the King Harvest alpine glacier complex or the LIS (Fig. 2B). The King Harvest alpine glacier deposited three easily identifiable and boulder-rich moraines: K1, K2, and K3 (Fig. 2B). The K1 moraine is the most distal and oldest alpine moraine within the sequence and is defined by a sharp right-lateral moraine crest. The next two King Harvest alpine moraines, K2 and K3, are slightly more subdued yet are characterized by full latero-frontal moraine ridges with an abundance of boulders (Fig. 2B).

The Okoa lateral moraine is a right lateral moraine deposited by LIS ice filling Okoa Bay (OL; Fig. 2B; Fig. 4A). Of particular interest are the valley floor (VF) and Narpaing lateral (NL) moraines that were deposited in the through-valley connecting Okoa Bay and Narpaing Fjord (Fig. 2B; Fig. 4B; Fig. 5). The orientations of Narpaing Fjord and the through-valley allow LIS ice in Narpaing Fjord to thicken and extend into the through-valley and thus both the VF and NL moraines are left lateral moraines deposited by LIS ice flowing down Narpaing Fiord (Fig. 4B). Briner et al. (2009) originally attributed the VF moraine to the King Harvest alpine complex based on analysis of aerial photographs. However, field observations by our team in 2015, which included original 2009 authors Briner and Miller, confirm that the VF moraine was deposited by LIS

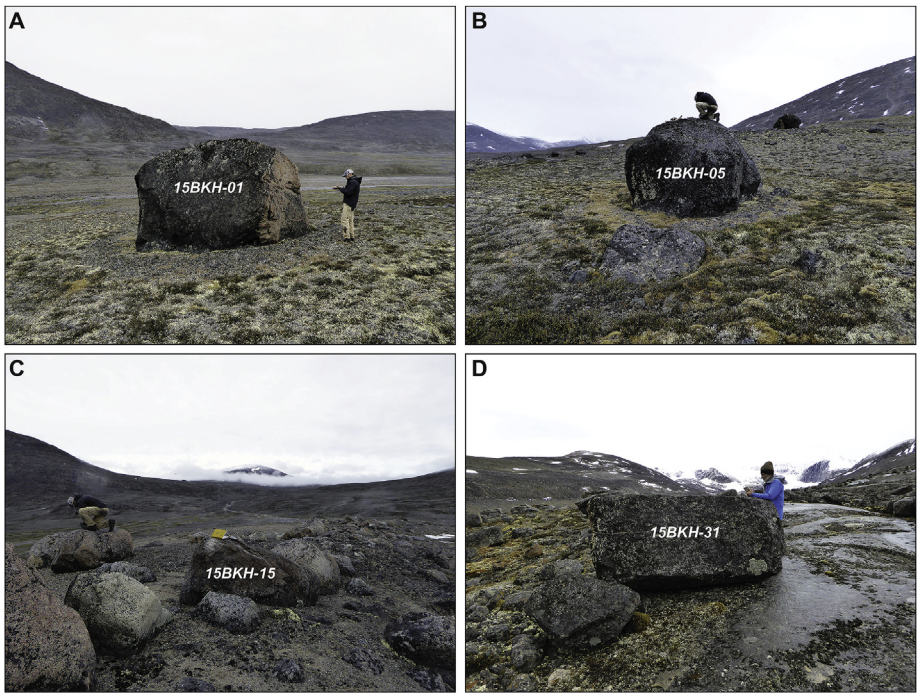

Fig. 5. (A) Sample 15BKH-01 with a ^{10}Be age of 25.48 ± 0.42 ka from the valley-floor (VF) moraine (Fig. 2B; Table 1); this sample has isotopic inheritance. (B) Sample 15BKH-05 from the VF moraine with an ^{10}Be age of 11.94 ± 0.25 ka. (C) Sample 15BKH-15 from the VF moraine with an ^{10}Be age of 11.73 ± 0.51 ka. (D) Example of a boulder perched directly on bedrock located upvalley of the King Harvest alpine moraines. Sample 15BKH-31 has a ^{10}Be age of 8.81 ± 0.18 ka.

ice emanating out of Narpaing Fjord. The VF moraine orientation is perpendicular to the K2 and K3 moraines and has a low-relief profile distinguishing the VR moraine from its K2 and K3 neighbors (Fig. 2B; Fig. 5; Fig. 6). In addition, the gradient of the through-valley connecting Okoa Bay and Narpaing Fjord routes King Harvest alpine ice to flow southeast towards Narpaing Fjord (and not towards Okoa Bay) as illustrated by the mapped King Harvest alpine moraines (Fig. 2B; K1, K2, K3 moraines). Based on field mapping, the K1 alpine moraine is truncated by the VF moraine as marked by a series of discrete lateral moraines resting between K1 and K2 that

Fig. 6. (A) Sample 15BKH-18 from the K2 moraine with a ^{10}Be age of 10.35 ± 0.37 ka. (B) View looking down the K1 lateral moraine crest towards Narpaing Fjord with sample 15BKH-36 (11.64 ± 0.23 ka). (C) Sample 15BKH-65 from the K3 moraine with a ^{10}Be age of 9.43 ± 0.18 ka. (D) View to the southeast with Narpaing Fjord in the background. Foreground shows sample 15BKH-68 from the K3 moraine with a ^{10}Be age of 11.62 ± 0.24 ka; this sample has isotopic inheritance.

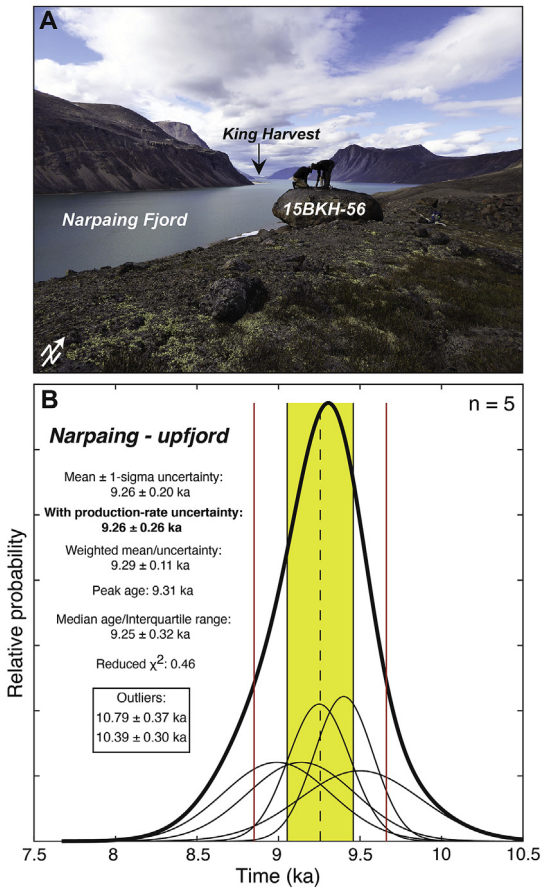

Fig. 7. (A) View looking down the crest of the upfjord moraine in Narpaing Fjord. Foreground: sample 15BKH-56 with a ^{10}Be age of 9.25 ± 0.19 ka. Background: opening to the King Harvest through valley. (B) Normal kernal density estimates for the Narpaing-upfjord moraine shown in panel A. Age in bold that includes the production-rate uncertainty is depicted in Fig. 17 and Fig. 18.

project to the main VF moraine sequence (Fig. 2B). In turn, these small VF lateral moraines are truncated by the K2 moraine. Based solely on the morphostratigraphic relationship between moraines displayed in the through valley, K1 is the oldest moraine, followed by the VF moraine, and the K2 and K3 moraines (Fig. 2B). Lastly, a prominent, sharp-crested, right-lateral moraine is located ~15 km from the King Harvest complex in Narpaing Fjord (Narpaing – upfjord; Fig. 2A). Because this lateral moraine is located upfjord of the King Harvest sequence, it is geomorphically younger than the NL moraine (Fig. 2A; Fig. 2B; Fig. 7A).

5.2. King Harvest ^{10}Be ages

Here, we present 61 ^{10}Be ages from the King Harvest moraine complex. Thirteen ^{10}Be ages from moraine boulders in the VF moraine complex range from 11.58 ± 0.22 ka to 25.48 ± 0.42 ka, 7 moraine boulders from the OL moraine range from 7.01 ± 0.17 ka to 19.12 ± 0.45 ka, and 7 moraine boulders from the NL moraine range from 10.21 ± 0.26 ka to 10.55 ± 0.20 ka (Fig. 2B; Fig. 8; Table 1). Seven ^{10}Be ages from moraine boulders on the Narpaing-upfjord moraine range from 8.99 ± 0.33 ka to 10.79 ± 0.37 ka (Fig. 2B; Fig. 8; Table 1).

In the King Harvest alpine moraine sequence, 6 ^{10}Be ages from boulders resting on the K1 moraine range from 11.64 ± 0.23 ka to 18.82 ± 0.62 ka, 7 boulders resting on the K2 moraine have ^{10}Be ages that span between 9.95 ± 0.24 ka to 27.71 ± 0.81 ka, and 10 moraine boulders on the K3 moraine have ^{10}Be ages between 4.74 ± 0.14 ka to 33.10 ± 0.63 ka (Fig. 2B; Fig. 8; Table 1). In addition, we sampled 4 boulders perched on bedrock located upvalley of the King Harvest alpine moraines; ^{10}Be ages for these 4 erratics are 8.89 ± 0.18 ka, 9.07 ± 0.18 ka, 9.15 ± 0.23 ka, and 9.32 ± 0.26 ka (Fig. 2B; Table 1).

5.3. Southwestern Greenland geomorphology

Six major moraine systems rest between the present coastline and the current GrIS margin in the Sisimiut-Kangerlussuaq region: Taserqat, Sarfartôq-Avatdleq, Fjord, Umîvît-Keglen, Ørkendalen, and Little Ice Age (LIA)-historical maximum (Fig. 3). In the broader Kangerlussuaq region, the GrIS margin currently either rests on the LIA-historical moraine, or at most has retreated a few 10s–100s of meters behind the LIA-historical moraine (Kelley et al., 2012; Levy et al., 2018), whereas all moraines located to the west of the LIA-historical moraine mark the episodic stillstand and/or readvance of the GrIS during overall ice-sheet recession in the early to middle Holocene (Weidick, 1974; van Tatenhove et al., 1996). These early Holocene moraine systems are not perfectly continuous and a single moraine crest cannot be traced through the entirety of our field area (Fig. 3). Regions of well-defined moraine crests are often separated by zones where moraines either thin to a patchy drift limit, or no moraines and/or drift are preserved at all. To distinguish between these two, our moraine mapping in Fig. 3 displays solid bold lines where moraines are well-defined, and dashed lines mark regions where moraine and/or drift limits are more ambiguous or are not preserved. We reiterate that our mapping follows that of Weidick (1974), with emphasis on distinguishing between moraine systems, and we only sampled boulders resting within regions where each moraine is well-defined.

While the ice-free landscape between the present coastline and the GrIS is dominated by the Taserqat, Sarfartôq-Avatdleq, Fjord, Umîvît-Keglen, and Ørkendalen moraine systems, their geomorphology differs. Our field observations and aerial surveys via helicopter reveal that the Sarfartôq-Avatdelq and Umîvît-Keglen moraines are the most continuous moraines preserved on the landscape. These moraine systems are typically characterized by uninterrupted moraine segments that are 10s of kilometers in length (Fig. 3). In contrast, the Taserqat Moraine, which is the westernmost and therefore oldest moraine on the landscape, is the most poorly defined moraine in the region (Fig. 3). The Taserqat Moraine is characterized by only sporadic segments of well-defined moraine crests, but we also note that Taserqat Moraine intersects a series of coastal inlets and fjords suggesting that this marine-based environment may in part contribute to the relative lack of moraine preservation (Fig. 3). In addition, we note the geomorphic difference between the Ørkendalen moraine complex versus the Taserqat, Sarfartôq-Avatdelq, Fjord, and Umîvît-Keglen moraine systems located to the west. In contrast to the Taserqat, Sarfartôq-Avatdelq, Fjord, and Umîvît-Keglen moraine systems, which primarily consist of well-expressed moraine crests with easily identifiable boundaries, the Ørkendalen moraine complex is defined by a continuous drift sheet that contains numerous small moraine crests. At the Ørkendalen type locality near the Russell Glacier, this drift limit extends ~2 km in front of the modern ice margin (Fig. 3; Weidick, 1974; Carrivick et al., 2017), whereas south of Russell Glacier, the Ørkendalen limit extends up to ~15 km in front of the ice margin near our ^{10}Be sample locations (Fig. 3; Weidick, 1974).

5.4. Southwestern Greenland ^{10}Be

We sampled boulders for ^{10}Be dating from each early or middle Holocene moraine in the GrIS forefield, but we primarily focused on

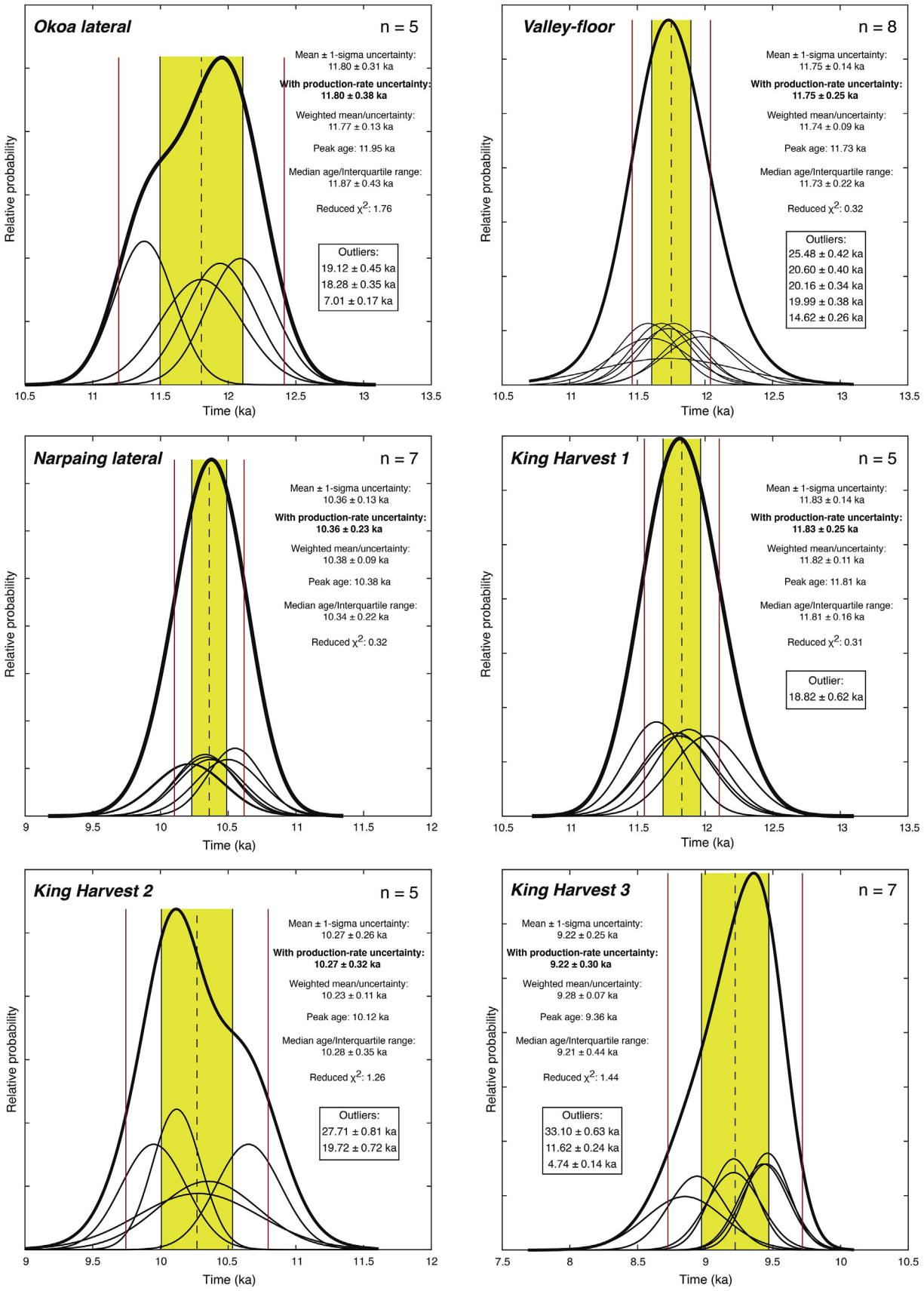

Fig. 8. Normal kernel density estimates for moraines in the King Harvest region. Ages in bold that include the production-rate uncertainty are depicted in Figs. 17 and 18.

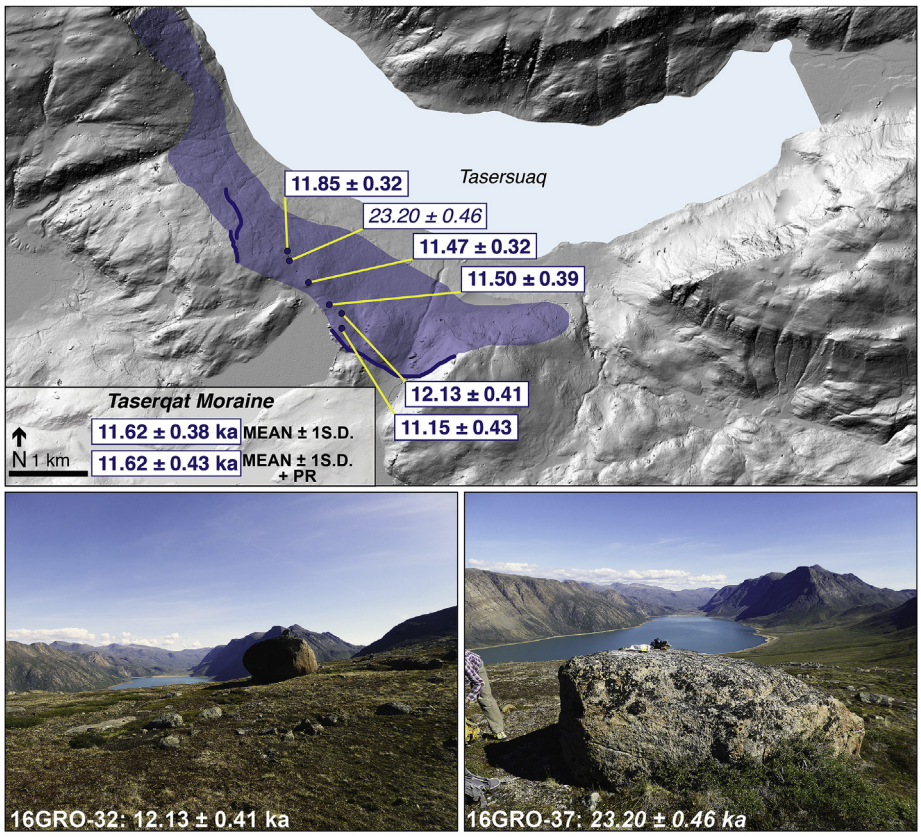

Fig. 9. Taserqat Moraine sample site with ^{10}Be ages and representative samples 16GRO-32 and 16GRO-37. Sample 16GRO-37 has isotopic inheritance.

constraining the ages of the Taserqat, Sarfartôq-Avatdelq, and Fjord moraines because previous efforts have focused on constraining the timing of deposition of the Umîvît-Keglen and Ørkendalen moraine systems near the town of Kangerlussuaq (Levy et al., 2012; 2018; Carlson et al., 2014; Winsor et al., 2015). Our 62 ^{10}Be ages from the region are distributed across the Taserqat (n = 6), Sarfartôq-Avatdelq (n = 14), Fjord (n = 9), Umîvît-Keglen (n = 5), and Ørkendalen (n = 6) moraine systems, and erratic boulders perched on bedrock beyond and between moraines (n = 19; Fig. 3A; Figs. 9–16). In addition, we dated 4 boulders resting on a minor recessional moraine crest located between the Fjord and Umîvît-Keglen moraines (Fig. 13). Six ^{10}Be ages from boulders on the Taserqat Moraine range from 11.15 ± 0.43 ka to 23.20 ± 0.46 ka (Figs. 9), and 14 ^{10}Be ages from moraine boulders distributed across two sites from the Sarfartôq-Avatdelq Moraine range from 10.12 ± 0.41 ka to 11.66 ± 0.42 ka (Fig. 10; Fig. 11). Nine ^{10}Be ages distributed across two sites from the Fjord Moraine span 8.84 ± 0.37 ka to 15.06 ± 0.41 ka (Fig. 12; Fig. 13), whereas 3 ^{10}Be ages from boulders resting on a minor recessional crest behind the main Fjord Moraine limit are 8.45 ± 0.24 ka, 8.66 ± 0.40 ka, 8.82 ± 0.27 ka (Fig. 13). Five ^{10}Be ages from boulders on the Umîvît-Keglen Moraine range from 7.93 ± 0.28 ka to 14.15 ± 0.60 ka (Fig. 13), and six ^{10}Be ages from Ørkendalen Moraine boulders range from 6.85 ± 0.24 ka to 7.72 ± 0.24 ka (Fig. 14). Our 19 ^{10}Be ages from boulders resting on bedrock range from 7.07 ± 0.20 ka to 14.21 ± 0.49 ka (Fig. 3A).

6. Developing ^{10}Be chronologies of ice-margin change

Here, we constrain the age of each moraine in the King Harvest region, Baffin Island, and on southwestern Greenland. Moraine ages

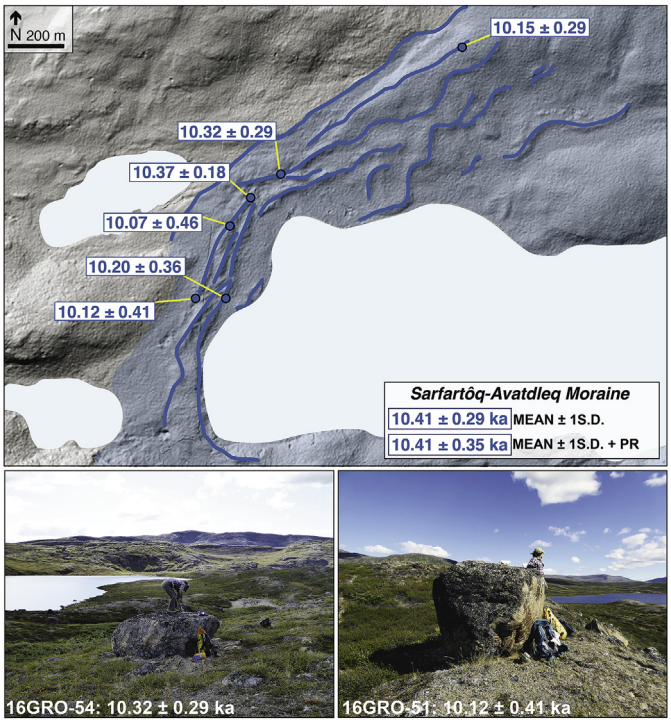

Fig. 10. Southern sampling site on the Sarfartôq-Avatdleq Moraine. This southern site comprises numerous well-defined moraine crests. Shown are representative samples 16GRO-51 and 16GRO-54.

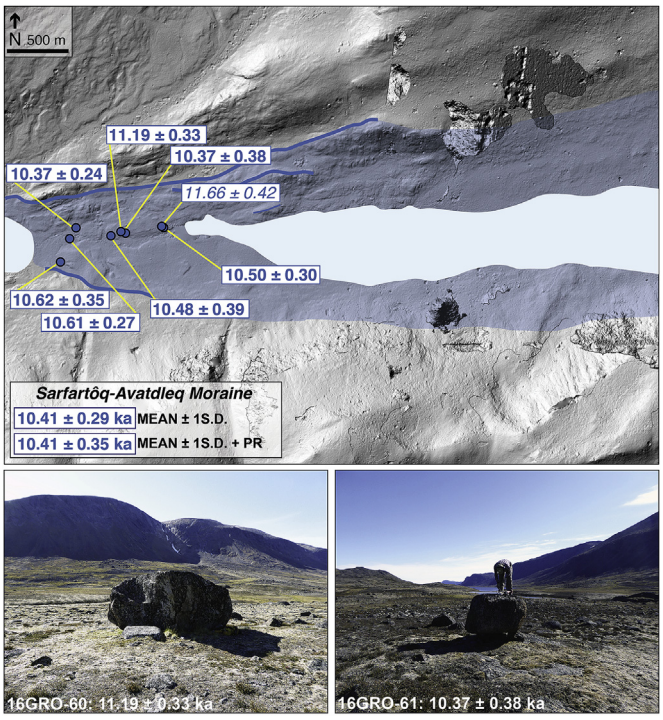

Fig. 11. Northern sampling site on the Sarfartôq-Avatdleq Moraine. Here the Sarfartôq-Avatdleq Moraine is mainly defined by a thin drift limit where patches of bedrock can be found among the drift. Shown are representative samples 16GRO-60 and 16GRO-61.

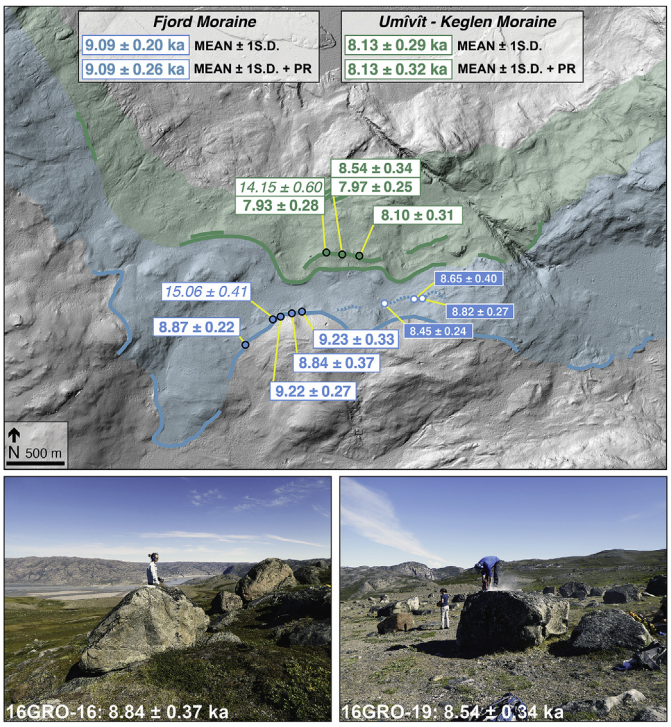

Fig. 13. Southern sampling site on the Fjord Moraine and the Umîvît-Keglen Moraine sampling site. Here, the Fjord and Umîvît-Keglen moraines are closely stacked, with a recessional moraine located between the two. We note that moraine ages at this location are in stratigraphic order. Shown are representative samples 16GRO-16 and 16GRO-19.

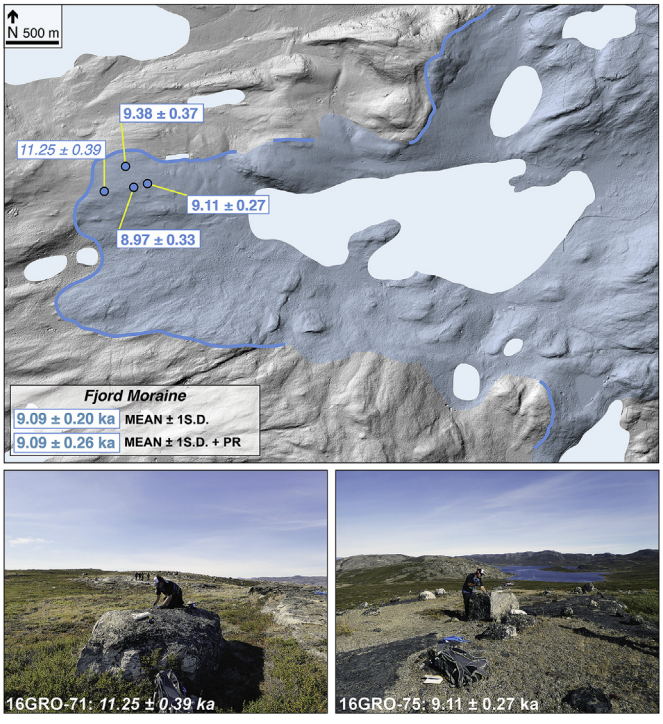

Fig. 12. Northern sampling site on the Fjord moraine. At the northern site, the Fjord Moraine thins to a well-defined drift limit where patches of bedrock can be found among the drift. Shown are representative samples 16GRO-71 and 16GRO-75 where bare bedrock can also be seen.

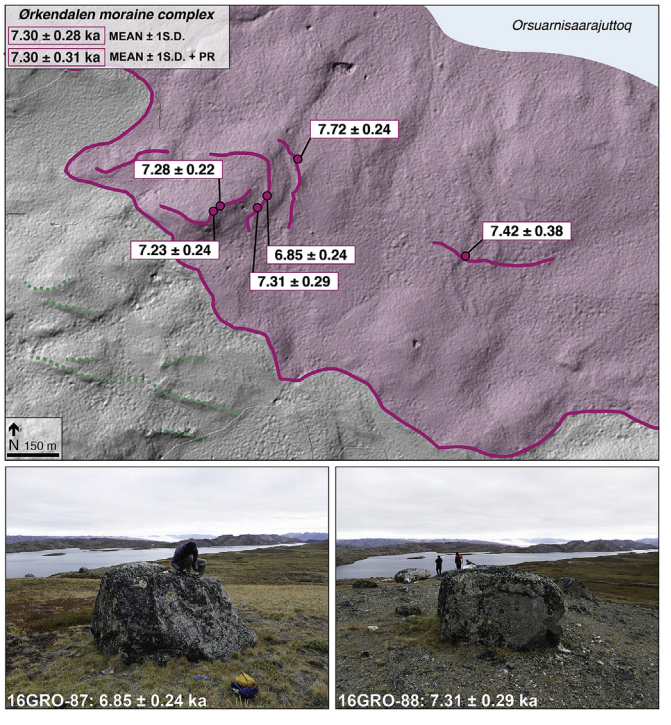

Fig. 14. Ørkendalen Moraine sample site with ^{10}Be ages and representative samples 16GRO-87 and 16GRO-88. These samples are from the outermost segment of Ørkendalen drift that is ~15 km from the modern ice margin. Located just beyond the Ørkendalen limit are minor recessional moraines (green dashed lines) that are part of the Umîvît-Keglen Moraine system.

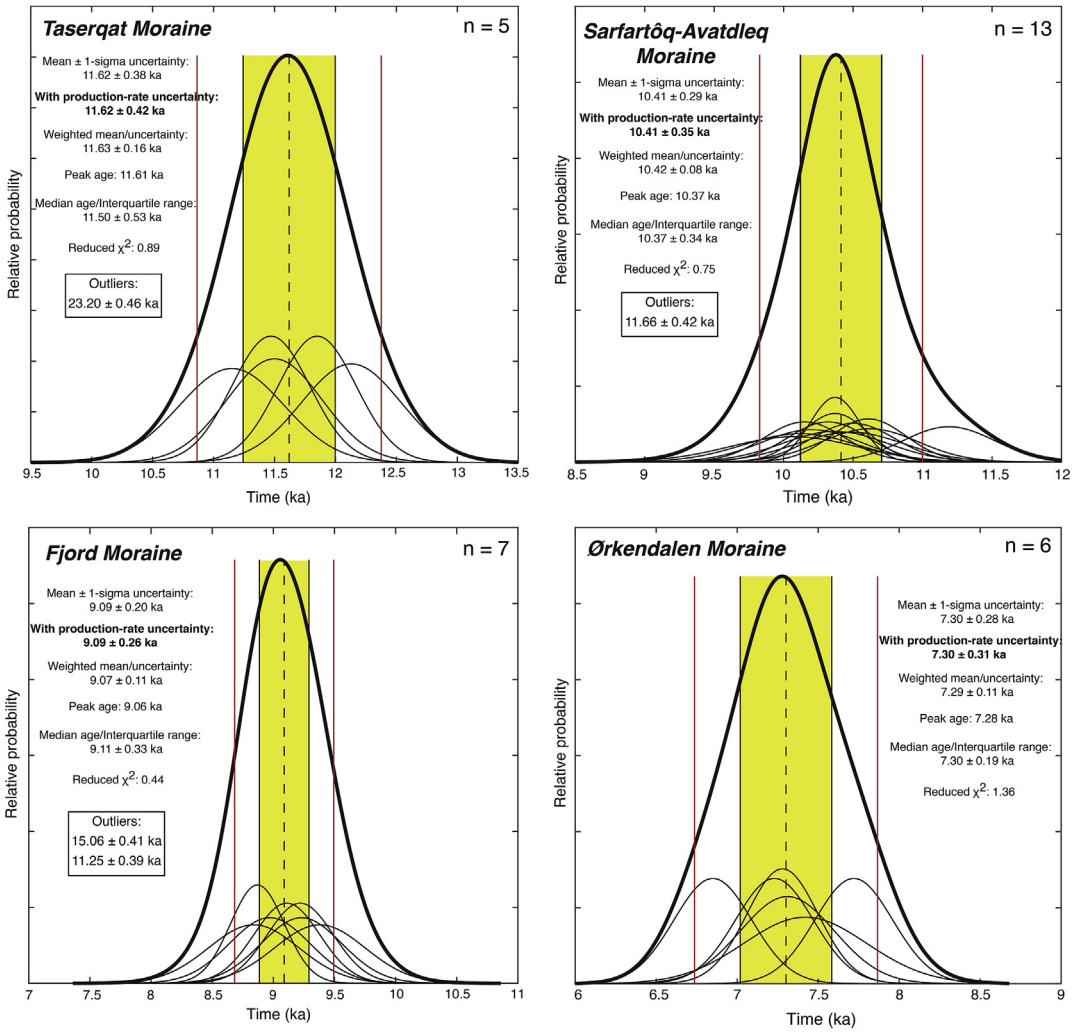

Fig. 15. Normal kernel density estimates for the Taserqat, Sarfartôq-Avatdleq, Fjord and Ørkendalen moraines (Table 1). Ages in bold that include the production-rate uncertainty are depicted in Figs. 17 and 18.

are expresses as the arithmetic mean ± 1 standard deviation (SD) of the ^{10}Be age population, not including outliers, which are discussed for each moraine. Outliers are defined as ^{10}Be ages that are >2SD older or younger from the mean ± 1 SD of the remaining ^{10}Be ages, or in two cases, defined by morphostratigraphic constraints. Moraine ages here do not include the uncertainty in the ^{10}Be production-rate calibration because we are only comparing ^{10}Be ages within King Harvest, southwestern Greenland, and across Baffin Bay. All of our ^{10}Be ages were calculated with the same ^{10}Be production-rate calibration dataset (Young et al., 2013a) and uncertainties in the production rate would result in systematic shifts in ^{10}Be age across all of our datasets and would not affect inter- and intra-site comparisons. When our moraine ages are compared to independent records of ice-sheet change or climate variability that are not on the ^{10}Be timescale, we include the uncertainty in the ^{10}Be production-rate calibration (Table 1). Our moraines ages simultaneously constrain the culmination of an advance or stillstand of a glacier or ice sheet and the timing of initial ice-margin retreat; moraine ages do not constrain the onset of an advance.

6.1. King Harvest ^{10}Be chronology

The oldest moraines deposited by the LIS in the King Harvest region are the OL and VF moraines (Fig. 2B; Fig. 8). Seven ^{10}Be ages on the OL moraine range from 7.01 ± 0.17 ka to 19.12 ± 0.17 ka, but 4 of these ^{10}Be ages cluster at 11.79 ± 0.32 ka after removing one younger outlier (7.01 ± 0.17 ka; Fig. 2B; Fig. 8; Table 1), and two older outliers that have ages of 19.12 ± 0.45 ka and 18.28 ± 0.35 ka (Fig. 2B; Table 1). The younger outlier likely reflects post-depositional exhumation of this moraine boulder, whereas the older two outliers are likely influenced by ^{10}Be inherited from a previous period of exposure (i.e. isotopic inheritance). The VF moraine was deposited at 11.75 ± 0.14 ka (n = 8) after excluding ^{10}Be ages of 25.48 ± 0.42 ka, 20.60 ± 0.40 ka, 20.16 ± 0.34 ka, 19.99 ± 0.38 ka, and 14.62 ± 0.26 ka (Fig. 2B; Fig. 8; Table 1). All of these outliers are significantly older than the 11.75 ± 0.14 ka cluster of ^{10}Be ages and likely contain isotopic inheritance. The NL moraine was deposited at 10.36 ± 0.13 ka (n = 7) and no outliers were identified in this ^{10}Be age population; all ^{10}Be ages from the NL moraine overlap at 1σ uncertainty (Fig. 2B; Fig. 8; Table 1). Lastly, the LIS deposited the Narpaing-upfjord moraine at 9.26 ± 0.20 ka (n = 5) after excluding two older ^{10}Be ages (Fig. 7B). These two older ^{10}Be ages are internally consistent and have ^{10}Be ages of 10.39 ± 0.30 ka and 10.79 ± 0.37 ka (samples 15BKH-60 and -61); including these ages would result in a bimodal age distribution for the Narpaing-upfjord moraine (Fig. 7B; Table 1). However, the

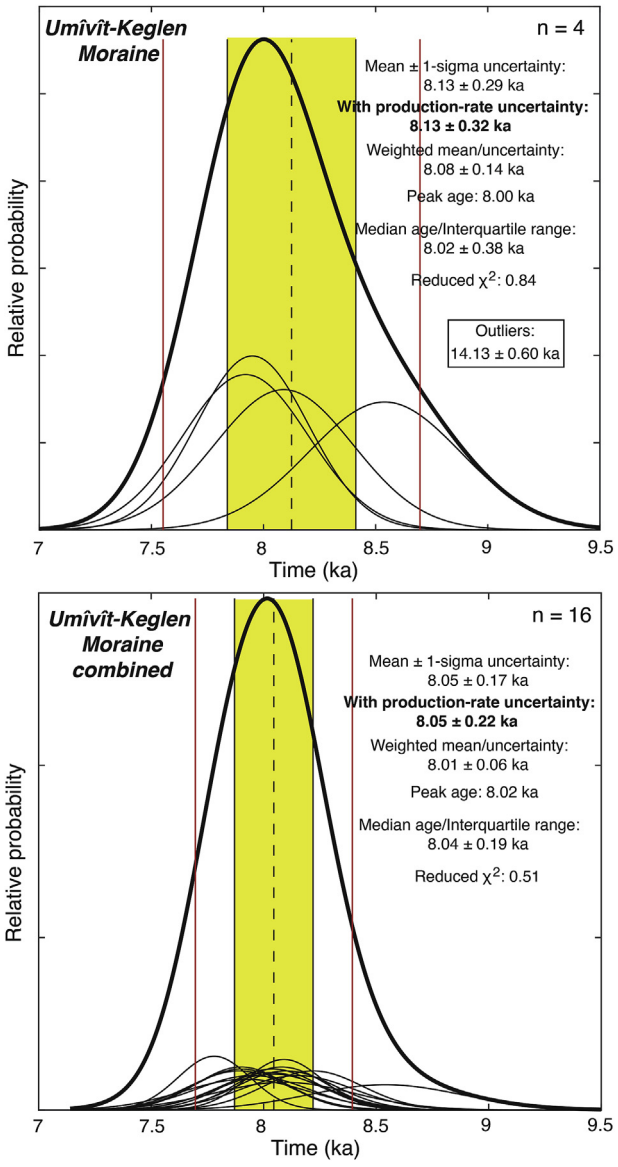

Fig. 16. Normal kernel density estimates for boulders on the Umîvît-Keglen Moraine from this study (top panel), and for boulders on the Umîvît-Keglen moraine from this study combined with Winsor et al. (2015) and Levy et al. (2018). We combine all three datasets to constrain the age of the Umîvît-Keglen Moraine to 8.05 ± 0.22 ka (n = 16).

Narpaing-upfjord moraine must be younger than the NL moraine in the King Harvest region, which was also deposited by the LIS outlet glacier occupying Narpaing Fjord and is tightly constrained to 10.36 ± 0.13 ka. Therefore, it is likely that ice in Narpaing Fjord quickly retreated after deposition of the NL moraine at 10.36 ± 0.13 ka, before re-advancing and potentially re-working samples 15BKH-60 and -61.

The oldest moraine deposited by the King Harvest alpine glacier complex (K1) was deposited at 11.83 ± 0.14 ka (n = 5) after excluding one older outlier that is likely influenced by isotopic inheritance (18.82 ± 0.62 ka; Fig. 2B; Fig. 8; Table 1). The K2 moraine was emplaced at 10.27 ± 0.25 ka (n = 5), again after excluding two older outliers that are likely influenced by isotopic inheritance (19.27 ± 0.42 ka and 27.71 ± 0.81 ka; Fig. 2B; Fig. 8; Table 1). The youngest alpine moraine, K3, was deposited at 9.21 ± 0.25 ka (n = 7) after removing 2 older outliers likely influenced by isotopic inheritance (11.62 ± 0.24 ka and 33.10 ± 0.63 ka; Fig. 2B Fig. 8; Table 1), and one younger outlier that almost certainly reflects boulder exhumation (4.74 ± 0.14 ka; Fig. 2B). Finally, 4 ^{10}Be ages from erratic boulders located up-valley and inboard of the King Harvest alpine moraines are 9.32 ± 0.26 ka, 8.89 ± 0.18 ka, 9.07 ± 0.18 ka, and 9.15 ± 0.23 ka (Fig. 2B; Table 1). These ^{10}Be ages are statistically identical and average 9.11 ± 0.18 ka, which is expected because post-depositional movement (e.g. exhumation; rotation) is unlikely for boulders resting directly on bedrock surfaces in tectonically stable environments. These upvalley ^{10}Be ages constrain the timing of valley deglaciation after deposition of the K3 moraine to 9.11 ± 0.18 ka, and also serves as a close minimum-limiting age for the K3 moraine independently dated to 9.21 ± 0.25 ka (Fig. 2B).

In summary, our ^{10}Be ages from across the King Harvest region reveal that LIS outlet glaciers deposited moraines at 11.79 ± 0.32 ka (OL), 11.75 ± 0.14 ka (VF), 10.36 ± 0.13 ka (NL), and 9.26 ± 0.20 ka (Narpaing-upfjord), whereas the King Harvest alpine glacier complex deposited moraines at 11.83 ± 0.14 ka (K1), 10.27 ± 0.25 ka (K2), and 9.21 ± 0.25 ka (K3), with valley deglaciation underway by 9.11 ± 0.18 ka (upvalley erratics). Based on mapping in the field, the K1 alpine moraine is truncated by the VF moraine suggesting that the VF moraine is geomorphically younger than the K1 moraine despite statistically identical ^{10}Be ages (Fig. 2B; Fig. 8; Table 1). We suggest that ice from the King Harvest alpine complex was resting on the through-valley floor before being overrun by LIS ice sourced from Narpaing Fjord, and it is possible that alpine ice may have briefly merged with LIS ice during deposition of the VF moraine. Regardless, ^{10}Be ages indicate that deposition of the VF and K1 moraines are statistically indistinguishable (Fig. 8).

Of the 61 ^{10}Be samples from the King Harvest region, 14 appear to be influenced by isotopic inheritance and only 2 are influenced by boulder exhumation (Fig. 2B; Table 1). This skew toward outliers containing isotopic inheritance could in part be reflective of an environment that contains cold-based to polythermal ice, which is inherently less erosive than warm-based ice. Or, the tendency towards outliers with isotopic inheritance could simply reflect the fact that, short of weathering pits in exposed rock surfaces, there are no obvious identifying characteristics for isotopic inheritance in the field that would aid in sample screening. The 14 ^{10}Be ages that appear to have isotopic inheritance, equates to ~23% of the total dataset, and two of these samples (10.39 ± 0.30 ka and 10.79 ± 0.37 ka) are from the Narpaing-upfjord moraine that is constrained to 9.26 ± 0.20 ka (Fig. 2A; Fig. 7; Table 1). The remaining 12 samples with isotopic inheritance are in the primary King Harvest moraine complex, and have ages that are significantly older than the remaining ages on each moraine (Fig. 2B; Table 1). Although inheritance affects a significant proportion of our dataset (23% of all samples), where present, inheritance is obvious and results in apparent ^{10}Be ages that are significantly older than the most likely moraine age; we are not faced with considering difficult-to-constrain trace amounts of inheritance (Table 1; Fig. 2B; Fig. 8; e.g. Kelly et al., 2008). The percentage of our samples influenced by isotopic inheritance is consistent with the overall percentage of low-elevation ^{10}Be ages (0–600 m asl) across Baffin Island that contain isotopic inheritance (~24%; n = 515; Young et al., 2016).

6.2. Southwestern Greenland ^{10}Be chronology

Sixty-two ^{10}Be ages from moraines and erratic boulders perched on bedrock constrain the timing and pattern of GrIS retreat through the early and middle Holocene (Fig. 3A). Three boulders perched on bedrock near the present coastline and outboard of all moraine systems have ages of 11.71 ± 0.54 ka, 11.60 ± 0.41 ka, and 11.13 ± 0.53 ka (Fig. 3A). These ^{10}Be ages overlap at 1SD, have a mean age of 11.48 ± 0.31 ka, and serve as a maximum age on the

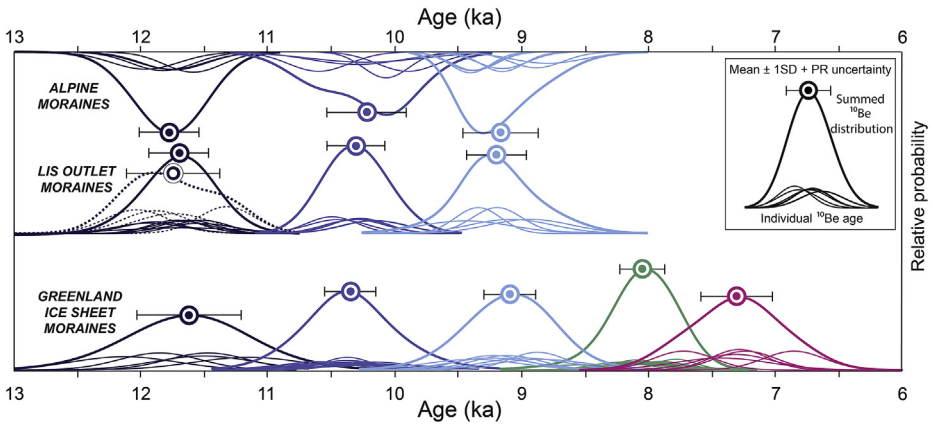

Fig. 17. Normal kernel density estimates for new ^{10}Be ages, excluding outliers, for moraines deposited by the by the King Harvest alpine glacier, LIS outlets, and the southwestern GrIS (Table 1). Including the ^{10}Be production-rate uncertainty, alpine moraines are dated to 11.83 ± 0.25 ka, 10.27 ± 0.32 ka, and 9.21 ± 0.30 ka. LIS outlet moraines are dated to 11.79 ± 0.38 ka, 11.75 ± 0.25 ka, 10.36 ± 0.13 ka, and 9.26 ± 0.20. GrIS moraines are dated to 11.62 ± 0.43 ka, 10.41 ± 0.35 ka, 9.09 ± 0.26 ka, 8.05 ± 0.22 ka (this study + Winsor et al., 2015 + Levy et al., 2018), and 7.30 ± 0.31 ka.

Taserqat Moraine (Fig. 3A). The Taserqat moraine was deposited at 11.62 ± 0.38 ka (n = 5), after excluding one older outlier (23.20 ± 0.46 ka; Fig. 15; Table 1). The one older outlier on the Taserqat Moraine with ^{10}Be age of 23.20 ± 0.46 ka is almost certainly influenced by isotopic inheritance and cannot accurately constrain the most recent period of exposure because the GrIS margin was likely somewhere out on the continental shelf at ~23 ka. Our moraine age is statistically identical to the age of the erratics located outboard of the Taserqat Moraine and suggest that deposition of the Taserqat Moraine occurred immediately after coastal deglaciation (Fig. 3A). We also note that our ^{10}Be ages from the outer coast and the Taserqat Moraine are consistent with the oldest minimum-limiting radiocarbon age from this region of 10.8 cal ka (Bennike et al., 2011).

The Sarfartôq-Avatdelq Moraine was emplaced at 10.41 ± 0.29 ka (n = 13) after excluding an older outlier of 11.66 ± 0.42 ka. Although this older outlier overlaps the mean ± SD of the remaining ^{10}Be age population at 2SD, we exclude the age 11.66 ± 0.42 ka based on morphostratigraphic constraints. Two ^{10}Be ages from erratics perched on bedrock located just outboard of the Sarfartôq-Avatdelq Moraine are 14.21 ± 0.49 ka and 10.76 ± 0.36 ka (Fig. 3A). Whereas the older of these two erratics is influenced by isotopic inheritance, the younger ^{10}Be age of 10.76 ± 0.36 ka places a firm maximum constraint on the age of the Sarfartôq-Avatdelq Moraine, and is also consistent with the age of the Sarfartôq-Avatdelq Moraine as constrained by ^{10}Be ages from moraine boulders. Moreover, the 11.66 ± 0.42 ka outlier is similar to ^{10}Be ages near the coast and from the geomorphically older Taserqat Moraine. Therefore, we exclude the ^{10}Be age of 11.66 ± 0.42 ka and calculate an age of 10.41 ± 0.29 ka for the Sarfartôq-Avatdelq Moraine. Three ^{10}Be ages from boulders perched on bedrock located ~20 km inboard (east) of the Sarfartôq-Avatdelq Moraine are 10.11 ± 0.34 ka, 9.61 ± 0.31 ka, and 9.61 ± 0.29 ka, and have a mean age of 9.78 ± 0.29 ka (Fig. 3A); this age acts as a minimum-limiting age for the Sarfartôq-Avatdelq Moraine. In addition, the suite of ^{10}Be ages on the Sarfartôq-Avatdelq Moraine marks the only instance in our dataset where ^{10}Be measurements from the same morphostratigraphic feature were made at LLNL-CAMS and PRIME. Sarfartôq-Avatdelq Moraine ^{10}Be measurements completed at LLNL-CAMS have a mean age of 10.36 ± 0.16 ka with 1σ measurement precision of 2.45 ± 0.46% (n = 5; Table 1), whereas ^{10}Be measurements completed at PRIME have a mean age of 10.44 ± 0.36 ka with 1σ measurement precision of 3.58 ± 0.56% (n = 8; Table 1).

Seven ^{10}Be ages from moraine boulders resting on the Fjord Moraine have a mean age of 9.09 ± 0.20 ka after excluding two older ^{10}Be ages of 11.25 ± 0.39 ka and 15.06 ± 0.41 ka that are likely influenced by isotopic inheritance (Fig. 12; Fig. 13; Fig. 15; Table 1). The age of 9.09 ± 0.20 ka for the Fjord Moraine as constrained by moraine boulders is consistent with the maximum-limiting age of 9.78 ± 0.29 ka (n = 3) as constrained by boulders perched on bedrock located outboard of the Fjord Moraine and inboard of the Sarfartôq-Avatdelq Moraine (Fig. 3A). In addition, north of Kangerlussuaq Fjord, two ^{10}Be ages of 9.59 ± 0.33 ka and 8.96 ± 0.31 ka from boulders perched on bedrock just beyond the Fjord drift limit are internally consistent and serve as another maximum constraint on the age of the Fjord Moraine. South of Kangerlussuaq Fjord, two additional ^{10}Be ages from boulders resting on bedrock outboard of the Fjord moraine are 9.56 ± 0.21 ka and 7.79 ± 0.19 ka. The ^{10}Be age of 9.56 ± 0.21 ka is likely an additional firm maximum-limiting age on the Fjord Moraine whereas the ^{10}Be age of 7.79 ± 0.19 ka is too young (Fig. 3A). There is no obvious explanation for this single younger age as exhumation or significant rotation of a boulder resting on bedrock is extremely unlikely, nor we did note any evidence of extensive sediment cover on the upper boulder surface. Lastly, a single ^{10}Be age of 9.38 ± 0.23 ka from a boulder perched on bedrock located south of Kangerlussuaq Fjord and inboard of the Fjord Moraine is a minimum-limiting age on the Fjord Moraine and is statistically identical to the age of the Fjord Moraine calculated from moraine boulders (9.09 ± 0.20 ka; Fig. 3A).

Four boulders from the Umîvît-Keglen Moraine have a mean age of 8.13 ± 0.29 ka after rejecting one older outlier that is likely influenced by isotopic inheritance (14.13 ± 0.29 ka; Fig. 3A; Fig. 13; Fig. 15; Table 1). In one location we obtained three ^{10}Be ages of 8.45 ± 0.24 ka, 8.65 ± 0.40 ka, and 8.82 ± 0.27 ka (mean age of 8.64 ± 0.19 ka) from a minor recessional moraine crest that is inboard of the Fjord moraine, but outboard of the Umîvît-Keglen Moraine (Fig. 13; Table 1). Our ^{10}Be ages from this recessional crest are consistent with their stratigraphic relationship between the ^{10}Be-dated Fjord and Umîvît-Keglen moraines in the same region, and likely constrain a brief stillstand of GrIS margin at 8.64 ± 0.19 ka.

The age of the Ørkendalen Moraine is constrained by six ^{10}Be ages from moraine boulders that all overlap at 1σ and have a mean age of 7.30 ± 0.29 ka (Fig. 3A; Fig. 14; Fig. 15; Table 1). Inboard of our moraine sampling site, 3 minimum-limiting ^{10}Be ages from boulders perched on bedrock are 7.07 ± 0.20 ka, 7.19 ± 0.20 ka, and 7.45 ± 0.24 ka, and consistent with the direct age of the Ørkendalen

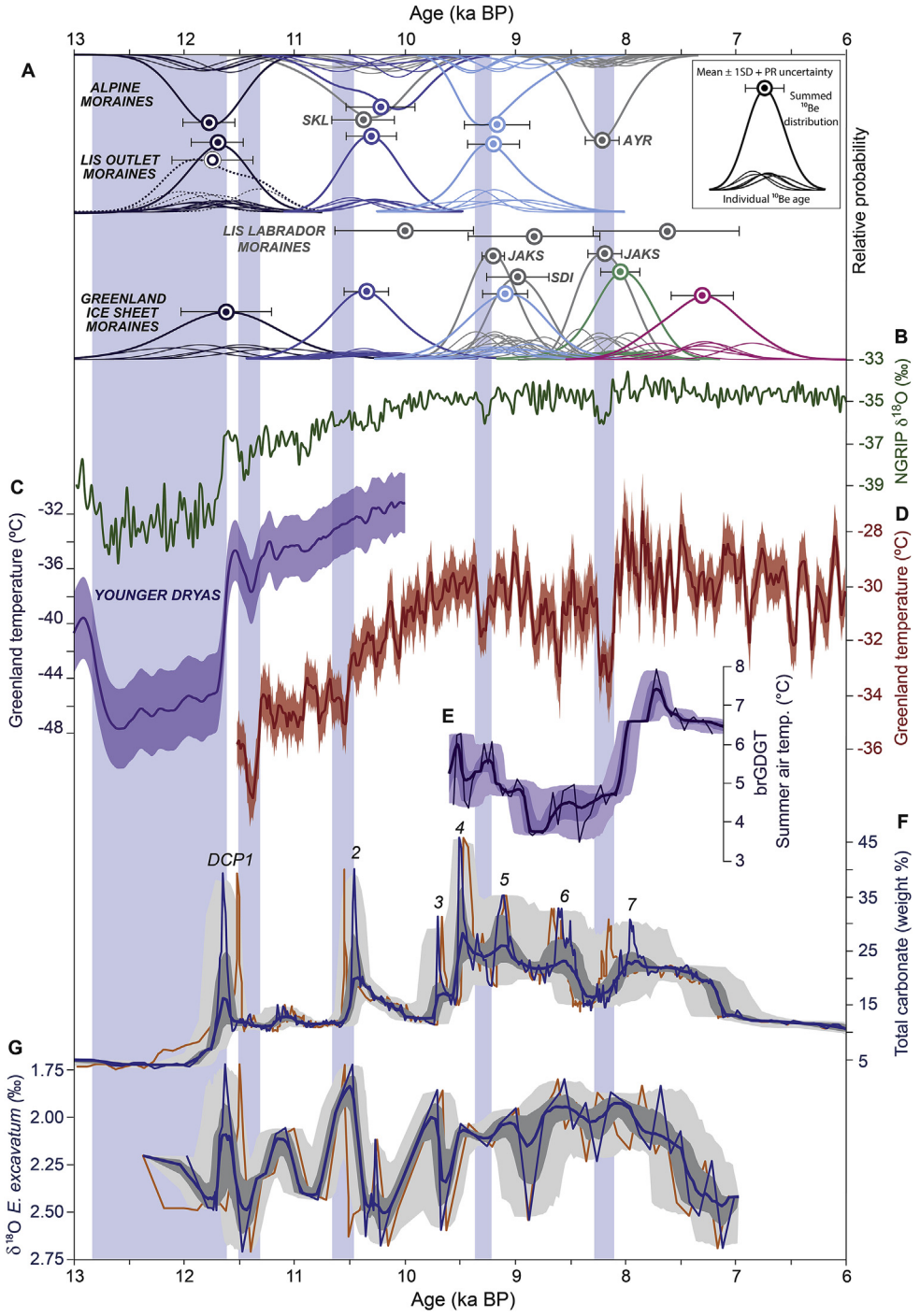

Fig. 18. (A) Same as Fig. 17 with the addition of previously published ^{10}Be-based moraine chronologies (lines and symbols in gray). Additional alpine moraines are dated to 10.39 ± 0.30 ka in western Greenland (Sikuiui Lake region; SKL; Fig.1; O'Hara et al., 2017) and 8.23 ± 0.21 ka on Baffin Island (AYR; Fig. 1; Young et al., 2012). Additional GrIS moraines are dated to 9.21 ± 0.19 ka and 8.20 ± 0.21 ka at Jakobshavn Isbræ (JAKS; Fig. 1; Young et al., 2011; Young et al., 2013a), and 8.99 ± 0.32 at Søndre Isortoq (SDI; Fig. 1; Table S1; Lesnek and Briner, 2018). Labrador moraines are dated to 9.99 ± 0.67 ka, 8.83 ± 0.63 ka, and 7.64 ± 0.75 ka (Ullman et al., 2016; Table S1) (B) δ^{18}O record from NGRIP ice core (Rasmussen et al., 2006). (C) Greenland mean-annual temperatures reconstructed using gas-phase $\delta^{15}N-N_2$ measurements (purple; ±1σ; Buizert et al., 2014). (D) Greenland mean-annual temperatures reconstructed using gas-phase $\delta Ar-N_2$ measurements (red; ±2σ; Kobashi et al., 2017). (E) Branched glycerol dialkyl glycerol tetraether-inferred summer temperature from Sikuiui Lake, western Greenland (Fig. 1; 70.218°N, 51.123°W, 604 m asl; Thomas et al., 2018). (F) Carbonate weight percentage from core MD99-2236 positioned on the Cartwright Saddle (Jennings et al., 2015; Fig. 1). DCP – detrital carbonate peak. (G) *E. excavatum f. clavata* δ^{18}O values from core MD99-2236 interpreted as freshwater input into the Labrador Sea (Jennings et al., 2015). The bold line in D, E, and F represents median value of our age-model iterations; the fine line represents each record on one age model; the dark and light gray shading represent the 1 and 2 sigma age uncertainty, respectively (McKay et al., 2018; McKay and Emile-Geay, 2016). The orange fine lines represent each record on the original age model of Jennings et al. (2015). Vertical blue bars are defined by the cooling events as expressed in Greenland ice core gas-phase temperature records.

moraine (Fig. 3A), and 3 ^{10}Be ages from just beyond Ørkendalen drift are 7.29 ± 0.17 ka, 7.59 ± 0.16 ka, and 9.00 ± 0.20 ka. Whereas the older age is likely influenced by isotopic inheritance, maximum-limiting ^{10}Be ages of 7.29 ± 0.17 ka and 7.59 ± 0.16 ka are consistent with the age of the Ørkendalen Moraine calculated from moraine boulders (7.30 ± 0.29 ka).

In summary, our ^{10}Be ages constrain deposition of the Taserqat Moraine to 11.62 ± 0.38 ka, Sarfartôq-Avatdelq Moraine to 10.41 ± 0.29 ka, Fjord Moraine to 9.09 ± 0.20 ka, Umîvît-Keglen Moraine to 8.13 ± 0.29 ka, and Ørkendalen Moraine to 7.30 ± 0.28 ka (Fig. 3A; Table 1). All of these moraine ages are further supported by a series of maximum- and minimum-limiting ^{10}Be from boulders perched on bedrock (Fig. 3A). Seven of our 62 ^{10}Be ages appear to have isotopic inheritance (Table 1) equating to ~11% of all Greenland boulder measurements. This value is slightly higher than the percentage of previously published low elevation (0–600 m asl) samples from southwestern Greenland with inheritance (~6%; n = 303; Young et al., 2016), but similar to the percentage of all southwestern Greenland ^{10}Be measurements that have isotopic inheritance regardless of sample elevation (~14%; n = 385; Young et al., 2016).

6.3. Integrating new and published ^{10}Be ages from southwestern Greenland

The landscape between the outer coast and current ice margin includes dozens of previously published ^{10}Be ages (Fig. 3B; Table S1). We discuss these existing ages within the context of our new ^{10}Be ages, and discuss, where appropriate, the integration of the two.

Rinterknecht et al. (2009) generated 12 ^{10}Be ages from a variety of features to produce a preliminary chronology of ice-margin recession and ice-sheet thinning (Fig. 3B). Four ^{10}Be ages from near the coast and outboard of the Taserqat and Sarfartôq-Avatdelq moraines range from ~19.6 ka to 106.5 ka (Fig. 3B). Two of these samples are from high-elevation bedrock surfaces where the presence of isotopic inheritance is more common (Table S1). It is possible that the most distal age of 19.62 ± 5.26 ka accurately reflects the timing of deglaciation at that site; however, because that sample is only ~140 m higher in elevation than our coastal samples, we suggest that the ~19.6 ka bedrock age does not accurately date GrIS recession, and instead is likely influenced by isotopic inheritance. Winsor et al. (2015) presented 9 ^{10}Be ages from near Sisimiut that range from 10.17 ± 0.60 ka to 37.59 ± 1.49 ka (Fig. 3B; Table S1). After attributing the older ages to inheritance and further suggesting that the 10.17 ± 0.60 ka age is too young, Winsor et al. (2015) suggested that the mean of 13.54 ± 1.01 ka, 14.44 ± 1.47 ka, and 15.25 ± 0.87 ka (14.41 ± 0.86 ka) constrains the timing of coastal deglaciation. However, these samples are ~80 m lower in elevation and are statistically older than our coastal ages of 11.71 ± 0.54 ka, 11.60 ± 0.41 ka, and 11.13 ± 0.53 ka (Fig. 3B). We suggest that these samples are influenced by a slight amount of isotopic inheritance and pre-date the timing of coastal deglaciation.

South of Kangerlussuaq fjord, Roberts et al. (2009) presented 16 ^{10}Be ages from a ridgeline elevational transect that range between 11.35 ± 0.42 ka and 165.8 ± 4.82 ka and span up to 856 m asl (Fig. 3B; Table S1). The goal of this study was to generate an ice-sheet thinning profile and each sample is from a bedrock surface, which increases the chances of isotopic inheritance (Table S1). A majority of these ages almost certainly contain isotopic inheritance, but we agree with the original interpretation of Roberts et al. (2009) that the lowest-elevation samples with ^{10}Be ages of 11.89 ± 0.48 ka and 11.35 ± 0.42 ka (Fig. 3B), accurately constrain the timing of coastal deglaciation. These two ages are statistically identical to our coastal ^{10}Be ages of 11.71 ± 0.54 ka, 11.60 ± 0.41 ka, and 11.13 ± 0.54 ka (Fig. 3B). Combined, these 5 coastal ^{10}Be ages average 11.54 ± 0.30 ka and serve as a minimum-limiting age on the submerged Hellefisk and Sisimiut moraine complexes offshore, and act as a closer limiting age on the Sisimiut moraine complex.

Farther inland, 8 additional ^{10}Be ages range from 7.63 ± 1.34 ka to 13.19 ± 1.67 ka (Rinterknecht et al., 2009). Notably, there is a cluster of ^{10}Be ages at ~9 ka from just beyond the Umîvît-Keglen limit, which is broadly consistent with our ice-margin chronology, but analytical uncertainties of up to 40% (mean = 16%) prevent including these ages within our ice-margin chronology (Fig. 3B). Several ^{10}Be ages from between the town of Kangerlussuaq and the modern ice margin directly relate to our newly generated ^{10}Be ages (Fig. 3B). Levy et al. (2018) and Winsor et al. (2015) directly, and independently, dated the Umîvît-Keglen Moraine in the same region to 8.04 ± 0.13 ka (n = 9) and 7.96 ± 0.11 ka (n = 3), respectively (Fig. 3B; Table S1). These two datasets are statistically identical and also indistinguishable from our age of 8.13 ± 0.29 ka (n = 4) generated from a different segment of the Umîvît-Keglen moraine (Fig. 3B). We combine all of these ^{10}Be ages to constrain deposition of the Umîvît-Keglen moraine to 8.05 ± 0.17 ka (n = 16; Fig. 16). This age is supported by a minimum-limiting radiocarbon age of 8.0 ± 0.2 (van Tatenhove et al., 1996), and also supports use of the Baffin Bay ^{10}Be production rate calibration dataset (Young et al., 2013a).

Near the Russell Glacier, Levy et al. (2012) and Carlson et al. (2014) independently dated Ørkendalen Moraine crests to 6.94 ± 0.42 (n = 7) and 6.76 ± 0.33 ka (n = 9), respectively, and Levy et al. (2018) presented three additional ages of 7.24 ± 0.20 ka, 7.03 ± 0.20 ka, and 7.02 ± 0.19 ka on boulders within Ørkendalen drift (Fig. 3B). Ørkendalen moraines in the Russell Glacier region have previously been constrained by radiocarbon to ~6.8 cal ka BP (van Tatenhove et al., 1996), consistent with ^{10}Be ages and further supports use of the Baffin Bay ^{10}Be production rate. Based on our own field observations, and also noted in the original mapping of Weidick (1974), our Ørkendalen moraine boulders (7.30 ± 0.28 ka; n = 6) come from a prominent moraine crest in region, whereas moraine crests in Russell Glacier region are minor, and interpreted as climatically insignificant recessional features. This geomorphic expression is consistent with the Ørkendalen Moraine system comprising a near continuous drift unit extending from ~2 km in front of the ice margin in the Russell Glacier region, to up to ~15 km beyond modern ice in our sampling region (Fig. 3B) resulting from relatively slow GrIS recession at this time. Because we interpret the.

Ørkendalen moraines as a near continuous drift unit, it is unlikely that the sampling of Levy et al. (2012) and Carlson et al. (2014) versus our sampling actually constrains the same ice limit and therefore identical ^{10}Be ages may not be expected. Thus, we do not combine our ^{10}Be ages with those Levy et al. (2012) and Carlson et al. (2014), but rather suggest that the GrIS was continuously depositing so-called Ørkendalen drift beginning at 7.30 ± 0.28 ka. Regardless, all three datasets place robust constraints on the timing of ice-margin recession through each sampling location. After deposition of the Taserqat, Sarfartôq-Avatdelq, Fjord, and Umîvît-Keglen moraines during the overall recession of the GrIS, the Ørkendalen system likely marks a significant slowdown of the ice margin resulting in a continuous drift sheet characterized by several small moraine crests and extensive sediment cover (e.g. Weidick, 1974; Carrivick et al., 2017).

7. Discussion

7.1. Synchronous response of the LIS and an alpine glacier to climate forcing

The close proximity of moraines in the King Harvest region that

were deposited by the LIS and alpine glacier complex allow us to assess the response of each ice mass to the same climate forcing; we do not expect climate to vary over such a small area on centennial time scales (Fig. 2B). Our ^{10}Be ages reveal LIS outlet moraines were deposited at 9.26 ± 0.20 ka, 10.36 ± 0.13 ka, 11.75 ± 0.15 ka (Narpaing Fjord) and 11.79 ± 0.32 ka (Okoa Bay), whereas King Harvest alpine moraines were deposited at 9.21 ± 0.25 ka, 10.27 ± 0.25 ka, and 11.83 ± 0.14. LIS outlet and alpine moraine ^{10}Be ages are statistically identical and, combined, these ^{10}Be ages indicate that advances and/or stillstands of the two LIS outlet glaciers peaked in tandem with advances of the King Harvest alpine glacier (Fig. 17). In summary, glacier advances at this site culminated at ~11.8 ka, ~10.3 ka, and ~9.2 ka (Fig. 2B; Fig. 17).

Alpine glaciers are sensitive to decadal-scale changes in temperature and precipitation (i.e. Oerlemans, 2005; Roe et al., 2017) and ice sheets also respond to climate change, but it is unclear if ice sheets are as sensitive to climate as alpine glaciers. For example, whereas ice sheets are thought to have long response times to climate (i.e. 'memory' or inertia) that range between several centuries to millennia depending on the magnitude of the climate perturbation (e.g., Applegate et al., 2014), relatively small alpine glaciers have comparatively short response times on the order of decades (Jóhannesson et al., 1989; Roe et al., 2017). Our results from the King Harvest region reveal that, at the very least, ice-sheet outlet glaciers respond to climate perturbations on the same centennial time scale as climate-sensitive alpine glaciers. However, the synchronous response of high-velocity outlet glaciers and alpine glaciers is perhaps to be expected. For example, modern observations suggest that high-velocity GrIS outlets are more sensitive to climate perturbations than their land-terminating neighbors (Bjørk et al., 2012; Kelley et al., 2012) Nonetheless, the synchronous deposition of King Harvest LIS and alpine moraines on several occasions in the early Holocene requires a climatic driver because it is unlikely that non-climatic fluctuations of each independent ice mass would result in repeated synchronous moraine deposition.

A moraine preserved on the landscape represents an unequivocal episode when an alpine glacier or ice sheet was more extended than today, and former alpine glacier dimensions are routinely used to reconstruct past climatic changes (i.e. Granger et al., 2013 and references therein). Yet, modelling exercises suggest that moraines found on the landscape need not be climatically significant as interannual variability may produce large fluctuations in glacier length and produce a moraine record that is unrelate to climate (Roe and O'Neal, 2009; Roe, 2011; Anderson et al., 2014). It appears that in the King Harvest region, however, each LIS outlet or alpine moraine preserved on the landscape has an equivalent counterpart indicating that each moraine is climatically significant. If deposition of synchronous LIS outlet glacier and alpine moraines requires a climatic driver, then our record of moraine deposition in the King Harvest region suggests that climate perturbations occurred at ~11.8 ka, ~10.3 ka, and 9.2 ka (Fig. 17).

7.2. Retreat of the Greenland ice sheet in southwestern Greenland

^{10}Be ages constrain deglaciation of the outer coast to 11.54 ± 0.30 ka (this study + Roberts et al., 2009), with moraine deposition occurring at 11.62 ± 0.38 ka (Taserqat), 10.41 ± 0.29 ka (Sarfartôq-Avatdleq), 9.09 ± 0.20 ka (Fjord), 8.05 ± 0.17 ka (Umîvît-Keglen; this study + Winsor et al., 2015 + Levy et al., 2018), and 7.30 ± 0.28 ka (outer Ørkendalen). Deglaciation of the landscape just beyond the modern and historical maximum limit occurred between ~7.3–6.8 ka as constrained by new and existing ^{10}Be ages near the modern ice margin (Fig. 8B; Levy et al., 2012; Carlson et al., 2014; Levy et al., 2018).

Our ^{10}Be-based chronology of ice-margin recession places firm constraints on the timing of moraine deposition, but we are largely unable to determine if moraine deposition occurred via a stillstand or readvance of the GrIS margin. However, statistically identical ^{10}Be ages from the Taserqat moraine (11.62 ± 0.38 ka) and the outer coast (11.54 ± 0.30 ka), indicate that deposition of the Taserqat moraine occurred via a stillstand of the ice margin (versus a re-advance; Fig. 3A). If ^{10}Be ages beyond the Taserqat moraine were ~13 ka (or older), the chronology would allow for the ice margin to retreat inland of Taserqat moraine at 13 ka, before re-advancing to deposit the Taserqat moraine at ~11.6 ka. In contrast, the actual ^{10}Be age distribution with identical ^{10}Be ages beyond the Taserqat moraine, and on the moraine itself, are suggestive of the Taserqat moraine being deposited during an ice margin stillstand (e.g. Young et al., 2013b). Thus, the GrIS margin in this region must also have been retreating prior to 11.6 ka as ice pulled out of Baffin Bay and made landfall.

Similar to the distribution of ^{10}Be ages from the outer coast and Taserqat moraine, a single maximum ^{10}Be age of 10.76 ± 0.36 ka is comparable to the age of the Sarfartôq-Avatdleq Moraine 10.41 ± 0.29 ka (Fig. 3A). This age distribution suggests that the Sarfartôq-Avatdleq Moraine was deposited during a stillstand of the GrIS margin during overall retreat. In addition, ^{10}Be ages of 9.59 ± 0.33 ka, 9.56 ± 0.21 ka, and 8.96 ± 0.31 ka from immediately outboard of the Fjord Moraine are similar the age of the Fjord moraine itself (9.09 ± 0.20 ka). Again, this ^{10}Be age distribution leaves little time for the GrIS margin to retreat inland of the Fjord moraine before readvancing to deposit the Fjord Moraine by 9.09 ± 0.20 ka, and suggests that the Fjord Moraine was deposited during a stillstand of the GrIS during overall retreat. South of Kangerlussuaq Fjord, our nested ^{10}Be ages of 9.09 ± 0.20 ka from the Fjord Moraine, 8.64 ± 0.19 ka from a recessional moraine, and 8.13 ± 0.29 ka from the Umîvît-Keglen Moraine are also suggestive of stillstands of the GrIS margin during gradual ice-sheet recession (Fig. 13). Lastly, we suggest that the Ørkendalen moraine system comprised of nearly continuous drift as opposed to well-defined ice limits, marks the stagnation, or perhaps minor readvances, of the GrIS beginning at 7.3 ± 0.28 ka and continuing to at least 6.9–6.8 ka (Levy et al., 2012; Carlson et al., 2014, Fig. 3B).

7.3. Synchronous ice sheet and glacier behavior in Baffin Bay

Moraine ages at the King Harvest site reveal that advances of the alpine glacier and neighboring ice sheet outlets occurred simultaneously at: 1) 11.83 ± 0.14 ka (alpine) 11.79 ± 0.32 ka (outlet), and 11.75 ± 0.14 ka (outlet), 2) 10.36 ± 0.13 ka (outlet) and 10.27 ± 0.26 ka (alpine), and 3) 9.26 ± 0.20 ka (outlet) and 9.21 ± 0.25 ka (alpine). These ages provide direct evidence for the synchronous response of LIS outlets and alpine glaciers to the same climate forcing in the Cumberland Peninsula region (Fig. 2B; Fig. 17; Table 1). Our moraine ages on Baffin Island are coeval with culminations of the GrIS occurring at 11.62 ± 0.38 ka, 10.35 ± 0.19 ka, and 9.09 ± 0.20 ka (Fig. 3B; Fig. 17; Table 1). Additional alpine moraines in western Greenland and on Baffin Island are dated with ^{10}Be to 10.39 ± 0.23 ka and 8.23 ± 0.15 ka (O'Hara et al., 2017; Young et al., 2012) and additional GrIS moraines in the Jakobshavn Isbræ forefield were deposited at 9.22 ± 0.10 ka and at 8.20 ± 0.15 ka (Young et al., 2011; Young et al., 2013a Fig. 18), which are coeval with the Fjord and Umîvît-Keglen moraines deposited at 9.09 ± 0.20 ka and 8.05 ± 0.22 ka (Fig. 18). Lastly, a land-terming sector of the GrIS at Søndre Isortoq, located south of our Sisimiut-Kangerlussuaq transect, deposited a prominent moraine at 8.99 ± 0.28 ka (Fig. 1; Fig. 18; Lesnek and Briner, 2018).

Our newly ^{10}Be-dated moraines from opposite sides of Baffin Bay, combined with published ^{10}Be-dated moraines point to

significant changes in regional climate at ~11.8–11.6 ka, ~10.4–10.3 ka, ~9.2–9.1 ka, and ~8.2 ka because we are unaware of any other mechanisms that can synchronize the behavior of so many independent ice masses (Fig. 17; Fig. 18). The correlation of ages from the King Harvest alpine moraines with LIS and GrIS moraines is robust. Uncertainties in ^{10}Be production rates may systematically alter absolute ages, but do not change differences between ages. Our data cannot discount the possibility that the behavior of Baffin Island and Greenland alpine glaciers, LIS and GrIS marine outlets, and the land-based GrIS margin were asynchronous on yearly to decadal timescales. On a centennial-scale, however, our ^{10}Be results are unequivocal; without the aid of complementary records of paleoclimate variability, synchronous repeated and linked changes of independent ice masses across Baffin Bay during the early Holocene are best explained by summer climate variations that occurred at ~11.8–11.6 ka, ~10.4–10.3 ka, ~9.2–9.1 ka, and ~8.2 ka.

Our ^{10}Be-based chronology of Baffin Bay moraines suggests that stabilization of alpine glaciers, the LIS, and the GrIS were a response to at least two known abrupt cooling events in the region. Well-known events centered at 9.3 ka and 8.2 ka are rapid multi-decadal to centennial-scale cooling events displayed in Greenland ice cores that were likely triggered by sudden outbursts of freshwater into the Labrador Sea region (Fig. 18; Barber et al., 1999; Rasmussen et al., 2007; Jennings et al., 2015). Synchronous response of Baffin Bay ice masses to the 9.3 and 8.2 ka cooling events has key implications regarding the primary mechanisms driving short-term ice-sheet behavior. An abrupt rise in temperature will force an ice sheet or alpine glacier margin to retreat off a moraine (Jóhannesson et al., 1989; Lowell et al., 1999), but the chronological link to the 9.3 ka and 8.2 ka cooling events presented here implies ice-sheet margin stabilization or readvance (and moraine deposition) in quick response to the cooling phase of an abrupt event. In Greenland ice cores, the 9.3 ka and 8.2 ka cooling events are ~40–100 years and ~160 years, respectively (Rasmussen et al., 2007; Thomas et al., 2007). Therefore, within the duration of these events, LIS outlet glaciers, and perhaps more notably the broad land-terminating margin of the GrIS, experienced a standstill or reversed overall retreat to readvance, deposit a moraine, and then retreat off that moraine at the end of each cooling event. An increase in precipitation can also force glacier advance, but increased snowfall in the accumulation zone must be propagated down-ice to the terminus, which, in the case of ice sheets, can take millennia (MacAyeal, 1993; Lowell et al., 1999). Increased precipitation in the terminus region can also affect the glacier balance ratio and lower the local equilibrium line altitude; more winter snowfall in the ablation takes longer to melt in the summer. However, the chronological link to known cooling events in which accumulation rates decrease (i.e. Rasmussen et al., 2007) suggest that ice sheet and glacier culminations at 9.3 ka and 8.2 ka are not precipitation driven. The synchronous advances of alpine glacier and ice-sheet termini centered at ~9.3 ka and 8.2 ka are therefore most likely facilitated by significantly reduced summertime melt rates in the ablation zone (e.g. Lowell et al., 1999).

7.4. Is the Baffin Bay record of ice-sheet change synchronous with the record of LIS change from the Labrador region?

Maybe. A number of ^{10}Be ages from the Labrador Dome region of the LIS also constrain the behavior of the LIS during the early Holocene (Ullman et al., 2016). Ullman et al. (2016) suggested that the Paradise, North Shore, and Sakami moraines were deposited at ~10.4 ka, 9.2 ka, and 8.2 ka, consistent with our ^{10}Be-dated moraines in Baffin Bay. However, ^{10}Be ages from the Labrador region were not calculated in a similar fashion as our ^{10}Be ages.

Rather than use the modern sample elevation to calculate a ^{10}Be age, Ullman et al. (2016) used a lower sample elevation to correct for the potential effects of isostatic rebound on ^{10}Be production. This correction resulted in ^{10}Be ages that are older than when ^{10}Be ages are calculated using the present-day elevation. In addition, Ullman et al. (2016) used the Northeastern North American ^{10}Be production-rate calibration dataset (NENA; Balco et al., 2009) which is statistically identical to the Baffin Bay calibration dataset (Young et al., 2013a). However, the calibration sites in both the NENA and Baffin Bay datasets have also experienced isostatic uplift. Logically, if an uplift correction is to be applied to calculate unknown ^{10}Be ages, that same uplift correction must be applied to the production-rate calibration dataset itself because the calibration sites have also undergone isostatic uplift. Then, the uplift-corrected production rate value must then be used when calculating unknown ^{10}Be ages. ^{10}Be ages for the Paradise, North Shore, and Sakami moraines were uplift-corrected, but calculated with the NENA ^{10}Be production rate that was not uplift corrected. The result of this age calculation method is that Ullman et al. (2016) report the oldest possible ^{10}Be ages for their samples.

The ages of the Paradise, North Shore, and Sakami moraines, when calculated in the same manner as we have calculated our Baffin Bay ^{10}Be ages (Baffin Bay production rate and no uplift correction; see Section 4.3.1) results in ages of 9.99 ± 0.67 ka (n = 8), 8.83 ± 0.61 ka (n = 10), and 7.64 ± 0.74 ka (n = 8; Table S1). Calculating these same ages using the uplift-corrected elevations of Ullman et al. (2016), and the Baffin Bay production rate that is not uplift corrected, results in ages of 10.13 ± 0.69 ka, 9.10 ± 0.62 ka, and 8.09 ± 0.79 ka. Young et al., 2013a also provided an uplift-corrected production rate which is 5.1% higher than the production rate that is not uplift corrected. Using the combination uplift-corrected Baffin Bay production rate and the uplift-corrected elevations and results in ^{10}Be ages that are 9.61 ± 0.69 ka, 8.63 ± 0.62 ka, and 7.68 ± 0.79 ka for the Paradise, North Shore, and Sakami moraines, respectively. These ages are similar to the ^{10}Be ages that are not uplift corrected. Despite ^{10}Be ages that are systematically younger than our Baffin Bay moraine ages, the uncertainties for the Paradise (9.99 ± 0.67 ka), North Shore (8.83 ± 0.61 ka), and Sakami moraines (7.64 ± 0.74 ka) allow these moraines to be plausibly correlated to our Baffin Bay moraine record (Fig. 18). Regardless of how the Labrador ^{10}Be ages are calculated, they demonstrate that the Labrador sector of the LIS deposited moraines approximately every 1 ka, consistent with our Baffin Bay record, and we suggest the most likely explanation is that deposition of the Paradise, North Shore, and Sakami moraines was contemporaneous with moraine deposition in Baffin Bay.

7.5. Ice sheet and glacier behavior in Baffin Bay and records of ice-rafted detritus and meltwater input from the Cartwright Saddle

The chronological link between freshwater forced cooling at ~9.3 ka and 8.2 ka as expressed in Greenland ice cores, and widespread glacier and ice-sheet response in Baffin Bay indicates that freshwater-forced cooling in the early Holocene is one mechanism that can drive widespread glacier and ice-sheet change. In addition to the 9.3 and 8.2 ka events, several other episodes of meltwater release from the LIS into the Labrador Sea likely occurred during the early Holocene (Jennings et al., 2015). Because of its position on the Cartwright Saddle, the presence of the southerly Labrador Current, and a carbonate IRD minerology, records of freshwater input and IRD from core MD99-2236 are interpreted as recording freshwater and IRD sourced from the Hudson Strait, which is the likely source region for 8.2 ka related meltwater and perhaps the 9.3 ka event (Fig. 18; Jennings et al., 2015). To gauge the relationship between our record of early Holocene glacier and ice-sheet stabilization and freshwater forcing, we compare our ^{10}Be dated records of ice-

margin change to an early Holocene record of freshwater input and ice rafted detritus (IRD) from the Cartwright Saddle in the Labrador Sea (MD99-2236; Jennings et al., 2015; Fig. 18).

Seven distinct IRD peaks occur between ~11.6 ka and 7.9 ka, each with a corresponding peak in freshwater input and, collectively, define a ~3.7 ka window of increased IRD and freshwater input into the Labrador Sea (Fig. 18; Jennings et al., 2015). Using an age model that is slightly modified from Jennings et al. (2015), the oldest IRD peak, DCP1, is centered at ~11.65 ka, followed by IRD peaks around 10.45 ka (DCP2), 9.70 ka (DCP3), 9.50 ka (DCP4), 9.10 ka (DCP5), 8.60 ka (DCP6), and 7.95 ka (DCP7). The hypothesis that the 9.3 ka and 8.2 ka cooling events are LIS freshwater-forced climate anomalies requires that freshwater input into the Labrador Sea precedes the cooling event. Within this context, Jennings et al. (2015) suggested that DCP4 and DCP7 correlate to the 9.3 ka and 8.2 ka cooling events (Fig. 18). On our modified timescale the DCP4 peak is centered at 9.50 ka and DCP1 at 7.95 ka. Whereas DCP4 does in fact precede the 9.3 ka cooling event and could represent the 9.3 ka event triggering mechanism, the timing of DCP7 post-dates the 8.2 ka event. However, in the original age-model of Jennings et al. (2015), DCP7 was centered at 8.2 ka (Fig. 18), and considering the age-model uncertainty, Jennings et al. (2015) interpreted DCP7 as marking the IRD/freshwater peak linked to the onset of the 8.2 ka event. Although DCP7 is centered at 7.95 ka on our age model, rather large age-model uncertainties allow the DCP7 peak to be older, and we agree with the original interpretation of Jennings et al. (2015) that DCP7 likely marks the final draining of Lake Ojibway resulting in the 8.2 ka event. In addition, we note that the age of a minor recessional moraine deposited by the GrIS at 8.64 ± 0.25 ka is statistically identical to the prominent peaks in IRD and meltwater at 8.60 ka recorded in core MD99-2236, and also identical to a cooling event recorded in Greenland gas-phase temperatures at this time (Fig. 18; Kobashi et al., 2017). We tentatively suggest that DCP6 and associated meltwater pulse marks an additional freshwater-forced cooling event recorded in Greenland gas-phase temperatures and our chronology of GrIS moraine deposition. Regardless, the IRD and meltwater records from core MD99-2236 on the Cartwright Saddle faithfully record the 9.3 ka and 8.2 ka event meltwater triggering episodes, whereas the subsequent cooling is clearly expressed in Greenland ice cores, and the culmination of this cooling is recorded in our ^{10}Be-based moraine record presented here (Fig. 18).

Using the 9.3 ka and 8.2 ka cooling events as a template, a pattern emerges: as meltwater sourced from the LIS enters the Labrador Sea, AMOC is likely reduced and triggers regional cooling expressed in Greenland ice cores, and this cooling leads to brief stillstands or readvances of the LIS, GrIS and alpine glaciers as seen in our moraine record. Within this context, the possible relationship between freshwater input into the Labrador Sea and summertime cooling in Baffin Bay centered at ~10.4 ka as defined by our ^{10}Be-based record is less clear. DCP2, centered on 10.45 ka (Jennings et al., 2015 age model = 10.50 ka) and accompanied by a significant input in freshwater is, within uncertainties, identical to ^{10}Be-based moraine ages from the LIS, GrIS and alpine glaciers in Baffin Bay. The consistency between the timing of ice-sheet and glacier stabilization in our record, and the timing of IRD and freshwater input into the Labrador Sea as recorded by MD99-2236 is suggestive of another freshwater forced cooling event centered on ~10.4 ka (Fig. 18). NGRIP δ^{18}O values, however, do not record an obvious cooling event at that time, but Greenland gas-phase temperatures reveal cooling centered at 10.5 ka (Fig. 18), and Bond et al. (1997) noted a significant peak in *Neogloboquadrina pachyderma* (sinistral) abundance from core VM29-191 in the North Atlantic Ocean. Cooling centered at ~10.5–10.4 ka, widespread ice sheet and glacier stabilization in Baffin Bay at ~10.4 ka, and a significant pulse in IRD and meltwater into the Labrador Sea through Hudson Strait is suggestive of meltwater-forced cooling event centered at 10.5–10.4 ka.

The link between regional cooling and ice-sheet/glacier culminations occurring at ~10.5–10.4 ka, 9.3 ka, and 8.2 ka necessitates that pulses in IRD and freshwater recorded in core MD99-2236 precede the cooling events themselves. Considering the uncertainties in the MD99-2236 chronology, the uncertainties in applied marine reservoir corrections, and the simple fact that pules in IRD represent inherent disconformities within MD99-2236 sediments (or any other sediment core) that skews any age-depth model, we suggest that each IRD/meltwater pulse does in fact precede the cooling events expressed in Greenland ice cores and our Baffin Bay moraine record. DCP2, DCP4, and DCP7 and their associated peaks in meltwater likely served as the triggering mechanism for regional cooling at ~10.5–10.4 ka, ~9.3 ka, and 8.2 ka, with perhaps an additional cooling event centered at ~8.6 ka (DCP6 and GrIS recessional moraine).

7.6. Freshwater forcing of early Holocene cooling events and ice sheet and glacier stabilization in Baffin Bay

The 8.2 ka cooling event represents perhaps the only abrupt cooling event where the relationship between freshwater and the cooling event itself is rather unambiguous: freshwater is released in some fashion into the Labrador Sea region leading to a reduction in AMOC strength and regional cooling which is clearly expressed in Greenland ice core records (e.g. Alley and Ágústsdóttir, 2005). Moreover, the meltwater source itself is widely considered to be Lake Ojibway along the former LIS southern margin (Barber et al., 1999; Clarke et al., 2004). Using these key constraints, considerable effort that has been made towards quantifying the amount, rate, and location of freshwater delivery into the Labrador Sea region that is responsible for the 8.2 ka event (e.g. Morrill et al., 2014 and references therein). These efforts can thus provide some estimates on the amount of freshwater input needed to drive coeval stabilization of Baffin Bay ice masses at 8.2 ka, and perhaps during other freshwater forced events.

Hydraulic modelling indicates that the final drainage of Lake Ojibway was characterized by the release of 2.5 Sv (0.79×10^4 m^3 or ~0.2 m sea-level equivalent) of water into the Labrador Sea region in <1 year, and typically serves as the initial meltwater input into the Labrador Sea for modelling efforts (Clarke et al., 2004; LeGrande and Schmidt, 2008; Wagner et al., 2013; Morrill et al., 2014). Whereas modelling exercises are generally able to reproduce the spatial distribution of climate anomalies associated with the 8.2 ka event when adding ~2.5–5 Sv freshwater to the Labrador Sea region, one key characteristic of most model runs is that the duration of the simulated climate anomaly is much shorter than the ~150 yr long 8.2 ka event as defined by Greenland ice cores (LeGrande and Schmidt, 2008; Wagner et al., 2013; Morrill et al., 2014). These simulations suggest that the location and magnitude of freshwater input exerts considerable control over simulated climate anomalies (Wagner et al., 2013; Morrill et al., 2014). It is possible that freshwater delivered into the Labrador Sea region would be confined to the coast (Condron and Winsor, 2011), but perhaps the most robust match between observed and simulated 8.2 ka climate anomalies occurs when freshwater is spread over a broad region in the Labrador Sea (Morrill et al., 2014). In addition, model simulations suggest that meltwater input from a Lake Ojibway discharge event alone is not able to force the century-scale reductions in AMOC strength needed for simulated 8.2 ka climate anomalies to match the duration of observed 8.2 ka anomalies (Wagner et al., 2013; Morrill et al., 2014). Rather, meltwater associated with the collapse of the Hudson ice dome is needed in addition to Lake Ojibway

sourced meltwater (Wagner et al., 2013). In one simulation, a total of 15.37 Sv (2.5 Sv + 0.13 Sv × 99 years) of freshwater input into the Labrador Sea results in a ~40% reduction in AMOC strength and, interestingly, this result is only sensitive to the amount of meltwater input and not the duration (Wagner et al., 2013). This magnitude of AMOC reduction is consistent with independent simulations that suggest ~50% reduction in AMOC strength results in the best match to climate proxy records (LeGrande et al., 2006; LeGrande and Schmidt, 2008). These simulations provide an estimate that AMOC weakening of perhaps up to 50% can reproduce the magnitude and duration of the 8.2 ka cooling event, which in turn can force the response of Baffin Bay ice masses presented here.

In comparison, very little targeted work has explored freshwater forcing for the 9.3 ka cooling event, which is similar in magnitude but shorter in duration than the 8.2 ka event. A possible first-order interpretation is that the 9.3 ka event may have simply involved a lesser amount of freshwater input into the Labrador Sea region than the 8.2 ka event if freshwater volume and not duration exerts a primary control on AMOC strength as suggested by recent 8.2 ka modelling exercises (Wagner et al., 2013). Fleitmann et al. (2008) suggested that the 9.3 ka event was triggered by ~0.26 Sv of meltwater input over 1 year, which is significantly less than the discharge from Lake Ojibway at the onset of the 8.2 ka event; however, 0.26 Sv should likely be considered a minimum value as the volume of meltwater from draining of Lake Ojibway alone (~2.6 Sv) cannot reproduce 8.2 ka climate anomalies (Wagner et al., 2013). Moreover, it is unknown if the magnitude of AMOC reduction during the 9.3 ka event was less than during the 8.2 ka event, or was similar (or more), but just lasted for a shorter period of time; the same can be said for possible freshwater forced cooling at ~10.5–10.4 ka (Fig. 18). In addition, background meltwater input from the LIS (i.e. Licciardi et al., 1999), and perhaps even the GrIS (i.e. Seidenkrantz et al., 2013), likely led to overall cooler baseline temperatures and reduced AMOC strength during the early Holocene, making it difficult to quantify the amount of freshwater discharge needed to perturb an already weakened AMOC (Renssen et al., 2009).

Despite unknown amounts of freshwater associated with the 9.3 ka event and cooling centered at ~10.5–10.4 ka, we emphasize their similarities with the 8.2 ka event: cooling recorded in Greenland ice cores, IRD and meltwater peaks sourced from the Hudson Strait, and widespread moraine deposition in Baffin Bay (Fig. 18). Cooling centered at ~10.5–10.4 ka need not have the same forcing mechanism as the 9.3 and 8.2 ka cooling events. Yet, given the similarities between all events in the proxy records considered here, we suggest that freshwater forcing is the most plausible mechanism for cooling at ~10.5–10.4 ka, and that this mechanism operated repeatedly during the early Holocene. In addition, repeated pulses in IRD and freshwater input between ~9.5 ka and 8 ka correspond to a significant centennial-scale cooling trend expressed at Summit Greenland and in a terrestrial record of summer temperature in western Greenland (Kobashi et al., 2017; Thomas et al., 2018; Fig. 18). Overall freshwater input into the Labrador Sea region between ~9.5 and 8 ka likely contributed to regionally cool baseline temperatures through this interval, punctuated by abrupt cooling events at ~10.5–10.4 ka, 9.3 ka, and 8.2 ka, and perhaps further aided by volcanic forcing (Renssen et al., 2009; Kobashi et al., 2017; Fig. 18).

The link between meltwater, ocean circulation, and regional cooling in the early Holocene has long been suspected as a key feature of the climate system of the North Atlantic region (Barber et al., 1999; Clark et al., 2001; Renssen et al., 2009). Our results extend this sequence: multi-decadal to centennial-scale cooling in response to freshwater forcing from the LIS and likely AMOC weakening in the early Holocene, drove the coeval stabilization of local alpine glaciers and ice sheets in Baffin Bay throughout deglaciation. However, a key feature of this hypothesis that freshwater input into the Labrador Sea results in regional cooling, is that expanded and/or prolonged winter sea ice in the region is the primary mechanism that drives cooler regional temperatures (i.e. Alley and Ágústsdóttir, 2005). Whereas expanded winter sea ice coverage in the North Atlantic Ocean is thought to drive extreme temperature seasonality with cooling primarily as a wintertime feature (i.e. seasonality hypothesis; Denton et al., 2005), coeval stabilization of local alpine glaciers and ice sheets in Baffin Bay requires reduced summer temperature (i.e. cooler melt season). Expanded wintertime sea ice likely drives extreme winter cooling with comparatively less cooling in the summer, but the two seasons and their relation to sea ice are not independent. Expanded winter sea ice will shorten the duration of the high-latitude melt season by taking longer to disappear in late spring or early summer, or the first formation of winter sea ice will occur earlier and potentially cut short the overall melt season. We suggest both scenarios would lead to a shortened melt season and reduced overall ablation.

7.7. Moraine deposition at the Younger Dryas termination and at ~7.3 ka

Our ^{10}Be-dated records of ice sheet and glacier change in Baffin Bay suggest a widespread period of moraine abandonment at ~11.8–11.6 ka (Fig. 17; Fig. 18), near the close of the Younger Dryas (YD; 12.9–11.7 ka), and an additional episode of moraine deposition by the GrIS at ~7.3 ka. Here we explore a few possible mechanisms that would lead to widespread moraine abandonment near the YD termination in Baffin Bay, and discuss the potential climatic relevance of the 7.3 ka GrIS moraine.

Widespread moraine abandonment at ~11.8–11.6 ka is coincident with a prominent IRD and freshwater peak at 11.65 ka (DCP1; Fig. 18), at end of the YD cold reversal. In comparison, the link between cooling and ice-margin stabilization centered at ~10.4 ka, 9.3 ka, and 8.2 ka requires an IRD/meltwater pulse that precedes the cooling event itself, which is permissible within the MD99-2236 age model (Fig. 18). The timing of IRD and meltwater influx into the Labrador Sea at the YD termination (DCP1; ~11.65ka) does not fit into the framework that DCP1 could be the YD triggering mechanism and precede the YD itself because is it unlikely that timing of DCP1 could realistically by shifted by at least 1.2 ka to the YD onset at ~12.9 ka (Fig. 18). Jennings et al. (2015) noted that DCP1, instead, likely marks the end of Younger Dryas and the retreat of ice through Hudson Strait, and therefore argued that IRD and associated meltwater can either occur near the onset or termination of a cooling event. One possibility is that DCP1, although occurring at the YD termination, is the triggering mechanism for the Preboreal Oscillation (PBO) centered at 11.4 ka and clearly reflected in Greenland ice core records. All our ^{10}Be-dated moraines overlap with the timing of the PBO at 1SD uncertainties, and would allow a scenario where DCP1 and associated meltwater serves as the PBO trigger, and our moraines were deposited in response to PBO cooling. Moreover, this scenario would be consistent with the chain of processes we propose for moraines deposited at ~10.5–10.4 ka, 9.3 ka, and 8.2 ka, and also consistent with the apparent response of GrIS outlets and an independent ice cap in eastern Greenland to the PBO (Levy et al., 2016). However, despite our moraine ages overlapping the PBO at 1-sigma uncertainties, our ^{10}Be ages are systematically older than the PBO, which likely precludes the link between Baffin Bay ice sheet and glacier behavior, the PBO, and DCP1 (Fig. 18).

Another possibility is that moraines in Baffin Bay dated to ~11.8–11.6 ka are “classical” YD moraines and mark a clear response to YD cooling; for example, moraines in Norway are interpreted to

date to the very end of the YD (Mangerud et al., 2016). The link between the 9.3 ka and 8.2 ka cooling events and our record of ice-sheet and glacier change in Baffin Bay indicates an almost immediate ice-sheet response to short-lived climate change (i.e. within dating resolution) that occurred on the order of several decades to under two centuries; simply put there is minimal lag time between the cooling event and ice-margin response. Thus, considering the demonstrated capacity of ice sheets and glaciers to respond to short-term cooling presented here at 9.3 ka and 8.2 ka, one might expect that any YD-related moraine would be deposited and abandoned early within the YD coinciding with peak YD cooling displayed in Greenland ice cores (Fig. 18). Because a ^{10}Be-dated moraine should simultaneously constrain the culmination of cooling and the initial rise in temperatures that forces an ice margin off its moraine, glacier advances should culminate early in the YD, followed by retreat through the YD (e.g. Vacco et al., 2009). In the Disko Bugt sector, the GrIS appears to have readvanced at ~12.2 ka followed by retreat through the remainder of the YD (Ó Cofaigh et al., 2013), and in southeastern Greenland, the GrIS also appears to have retreated through the YD (Rainsley et al., 2018). In the eastern North Atlantic region, the Loch Lomond Readvance culminated between ~12.8 ka and ~12.6 ka (Bromley et al., 2018), and advances of the western margin of the Scandinavian ice sheet culminated in many areas during the early or middle YD (Briner et al., 2014). Moreover, a ^{10}Be-dated moraine sequence from the Pacific sector also indicates that the YD advance of alpine glaciers culminated early in the YD followed by glacier recession (Young et al., 2019). Yet, our moraine ages of ~11.8–11.6 ka in Baffin Bay do not fit this pattern of glacial culminations occurring early within the YD and coincident with peak YD cooling.

An alternative explanation merges the hypothesis of ice-sheet retreat through the YD and a brief episode of freshwater-forced cooling near the YD termination. First, we note that identical ^{10}Be ages from the Taserqat Moraine and from erratics located outboard of the moraine in western Greenland requires that the GrIS margin was retreating prior to moraine deposition at the YD termination, and that moraine deposition likely occurred via a brief stillstand of the ice margin (Fig. 3A; Section 7.2). Therefore, overall net retreat of the GrIS margin was only briefly interrupted by regional cooling and moraine deposition near the YD termination, and the Taserqat Moraine does not represent the culmination of a prolonged YD cool interval. We suggest that widespread moraine deposition in Baffin Bay at the YD termination marks a brief episode of cooling that interrupted overall late YD warming. In this scenario, retreat of the LIS and GrIS through the YD is halted by the injection of freshwater associated with DCP1, which, in turn triggers regional cooling and brief stillstand of the LIS and GrIS. In addition, this hypothesis would offer a consistent mechanism that drives stabilization of Baffin Bay ice masses at ~11.8–11.6 ka, ~10.4 ka, 9.3 ka, and 8.2. ka, which is fully allowable when considering the uncertainties in ^{10}Be ages and the MD99-2236 age model (Fig. 18). We do note, however, that this scenario linking DCP1 and moraines dated to ~11.8–11.6 ka would require low-elevation regional cooling because a clear cooling episode is not reflected in Greenland ice cores at this time (Fig. 18). Alternatively, the cooling affecting a brief ice margin halt is a summertime feature whereas the major shift at ice core sites involves significant winter warming that obscures the climate change we propose. Additionally, Summit Greenland ice core sites receive a majority of their moisture from the eastern North Atlantic region suggesting that changes in source water δ^{18}O or temperature in the Labrador Sea region may not be recorded in Greenland ice cores (Sodemann et al., 2008). Thus, brief cooling in the Baffin Bay region at the YD termination, perhaps triggered by meltwater, is confined to the region, but does not have the hemispheric signature that the 9.3 ka and 8.2 ka events do, which are recorded not only in Greenland ice cores, but in Asian speleothem records (e.g. Dykoski et al., 2005).

The Ørkendalen Moraine dated to 7.30 ± 0.31 ka does not have a clear link to changes in temperature, IRD or meltwater in the Baffin Bay region (Fig. 18). Greenland ice core gas-phase temperatures suggest an episode of cooling centered at ~7.3 ka that interrupts overall warmer temperatures (Fig. 18). In addition, a slight freshening of the Labrador Sea at ~7.3 ka is recorded at the Cartwright Saddle yet no pulses in IRD accompany this pulse in meltwater (Fig. 18), although injections of freshwater need not be accompanied by IRD. It is possible that deposition of the Ørkendalen Moraine system is linked to regional cooling, but unlike other modes of moraine deposition in our Baffin Bay record, there are no additional moraines deposited by other sectors of the GrIS, LIS or regional alpine glaciers dated to ~7.3 ka (Fig. 18). Unlike modes of moraine deposition at ~11.8–11.6 ka, ~10.4 ka, ~9.3 ka, and 8.2 ka in Baffin Bay, we cannot argue that deposition of the Ørkendalen system beginning at ~7.3 ka clearly represents a regional change in summer climate. Yet, similar to the expression of the 9.3 ka and 8.2 ka events, a prominent climate anomaly at ~7.2 ka is also clearly expressed in Asian speleothem records and is linked to high-latitude temperature change (Feng et al., 2019). Nonetheless, based primarily on the geomorphology of the Ørkendalen Moraine system, which is characterized as a continuous drift sheet, the Ørkendalen Moraine system may simply represent a slowing or stagnation of the GrIS ice margin beginning at ~7.3 ka and continuing until at least 6.9–6.8 ka (i.e. Levy et al., 2018).

8. Conclusions

123 new ^{10}Be ages from Baffin Island and southwestern Greenland constrain the early Holocene behavior of two LIS outlets, the southwestern margin of the GrIS, and an independent alpine glacier. Our new dataset reveals:

- Advances of LIS outlets in the King Harvest region, Cumberland Peninsula, culminated at 11.79 ± 0.38 ka (Okoa Bay), 11.75 ± 0.25 ka (Narpaing Fjord), 10.36 ± 0.23 ka, and 9.26 ± 0.26 ka. Advances of the King Harvest alpine glacier culminated at 11.83 ± 0.25 ka, 10.27 ± 0.32 ka, and 9.21 ± 0.30 ka
- Synchronous moraine deposition of LIS outlets and an alpine glacier in the King Harvest region indicates both ice masses responded in unison to the same climate forcing.
- In southwestern Greenland, overall net retreat of the GrIS margin was interrupted by likely ice-margin stillstands culminating at 11.62 ± 0.43 ka (Taserqat Moraine), 10.41 ± 0.35 ka (Sarfartôq-Avatdleq Moraine), 9.09 ± 0.26 ka (Fjord Moraine), 8.05 ± 0.22 ka (Umîvît-Keglen Moraine), and 7.30 ± 0.31 ka (Ørkendalen Moraine). Our chronology of GrIS ice-margin recession in the early Holocene provides a firm set of benchmarks for geophysical ice-sheet models aiming to accurately simulate the evolution of the GrIS.
- Our new ^{10}Be ages, combined with published ^{10}Be ages from moraines in the Baffin Bay region indicate that the LIS, GrIS and alpine glaciers advanced and/or paused during overall net retreat at ~11.8–11.6 ka, 10.4 ka, 9.3 ka, and 8.2 ka, suggesting that Baffin Bay ice masses responded in unison to a common climatic driver. Our results also indicate that high-velocity LIS and GrIS outlet glaciers and low-velocity land-terminating sectors of the GrIS are both capable to responding to short-lived cooling.
- Moraines dated to ~11.8–11.6 ka in Baffin Bay reveal that Baffin Bay ice masses temporarily stabilized near the YD termination. We suggest coeval stabilization of Baffin Bay ice masses at ~11.8–11.6 ka was in response to an episode of brief freshwater-

forced regional cooling that interrupted overall warming near the YD termination.

The Baffin Bay moraine record, the record of LIS-sourced meltwater pulses provided by MD-2236 on the Cartwright Saddle, and temperatures from Summit Greenland point to the consistent freshwater forcing of early Holocene cooling events via the LIS at ~10.5–10.4 ka, 9.3, and 8.2 ka. In addition, our record identifies the widespread stabilization of Baffin Bay ice sheets and glaciers at ~11.8–11.6 ka, near the YD termination. We suggest that overall disintegration of ice sheets in the early Holocene (i.e. Dyke, 2004) began a self-regulating negative feedback mechanism: Laurentide ice sheet-derived meltwater discharged into the Labrador Sea region likely weakened AMOC which, in turn, lowered regional temperature and triggered repeated pauses or re-advances of the LIS, southwestern GrIS margin, and regional alpine glaciers (Fig. 17; Fig. 18). Within this context, the 8.2 ka event serves as the template for freshwater-forced cooling that resulted in ice-sheet stabilization during net ice-sheet recession, and we suggest this same chain of events occurred at ~10.5–10.4 ka and 9.3 ka. It is possible that cooling centered at 10.5–10.4 ka, and perhaps even 9.3 ka, may not be freshwater-forced events, but in the key proxy records considered here, these events share the same characteristics as the 8.2 ka event (Fig. 18). If cooling at ~10.5–10.4 ka and 9.3 ka is not freshwater forced, then an alternative mechanism must be invoked to trigger widespread cooling at ~10.5–10.4 ka and 9.3 ka as marked by our Baffin Bay moraine record, followed by a switch to the freshwater-forced 8.2 ka cooling event.

A lack of a rapidly melting LIS and large proglacial lakes almost certainly precludes the sudden collapse of modern AMOC (Clark et al., 2008), but observations coupled with modelling exercises suggest that meltwater produced by the modern GrIS is beginning to freshen Labrador Sea surface water (Bakker et al., 2016; Böning et al., 2016). Moreover, it is hypothesized that enhanced GrIS melt is contributing to observed 20th century slowdown of AMOC and decadal-scale cooling in the North Atlantic region (Rahmstorf et al., 2015), and that increasing GrIS melt may be contributing to centennial-scale AMOC weakening over the last ~150 years (Thornalley et al., 2018). In perhaps an extreme scenario, model simulations suggest a 75% reduction in AMOC strength or even AMOC collapse by CE 2300 when including realistic GrIS melt rates (Bakker et al., 2016). The geological record of ice-sheet variability in Baffin Bay presented here suggests that the last time AMOC significantly weakened, the LIS and GrIS paused or re-advanced during overall net retreat in a warming climate. These results suggest that slow or paused ice-sheet retreat due to meltwater-triggered cooling is an inherent feature of a deglaciating ice sheets in Baffin Bay. Whereas significant GrIS deglaciation, and perhaps runaway retreat, is expected over the upcoming centuries to millennia (Robinson et al., 2012; Applegate et al., 2014), reduction in AMOC driven by increased GrIS meltwater may provide a mechanism for multi-decadal scale regional cooling and brief stabilizations of the GrIS margin during overall net recession.

Acknowledgments

We thank A. Cluett, M. Koppes, M. Turrin, and H. Roop for help in the field, the 109th Airlift Wing for transport to Greenland, CPS for logistical support, and Air Greenland for helicopter support. We also thank R. Schwartz, J. Hanley and J. Frisch for help processing ^{10}Be samples. Funding was provided by the National Science Foundation Arctic Natural Sciences program (Awards #1417675 to NEY and JMS; #1417783 to JPB; #1418040 to GHM). ^{10}Be measurement data are housed at the NSF Arctic Data Center: doi:10.18739/A27M0409J. We thank 5 anonymous reviewers who provided comments on this manuscript. This is Lamont-Doherty Earth Observatory contribution #8368 and LLNL-JRNL-798584.

Appendix A. Supplementary data

Supplementary data to this article can be found online at https://doi.org/10.1016/j.quascirev.2019.106091.

References

Alley, R.B., Ágústsdóttir, A.M., 2005. The 8k event: causes and consequences of a major Holocene abrupt climate change. Quat. Sci. Rev. 24, 1123–1149.
Alley, R.B., Mayewski, P.A., Sowers, T., Stuiver, M., Taylor, K.C., Clark, P.U., 1997. Holocene climatic instability: a prominent, widespread event 8200 yr ago. Geology 25, 483–486.
Anderson, L.S., Roe, G.H., Andersen, R.S., 2014. The effects of interannual climate variability on the moraine record. Geology 42, 55–58.
Andrews, J., Ives, J., 1978. Cockburn nomenclature and the late quaternary history of the eastern Canadian Arctic. Arct. Alp. Res. 10, 617–633.
Applegate, P.J., Parizek, B.R., Nicholas, R.E., Alley, R.B., Keller, K., 2014. Increasing temperature forcing reduces the Greenland Ice Sheet's response time scale. Clim. Dyn. 45, 2001–2011.
Bakker, P., Schmittner, A., Lenaerts, J.T.M., Abe-Ouchi, A., Bi, D., van den Broeke, M.R., Chan, W.-L, Hu, A., Beadling, R.L., Marsland, S.J., Mernild, S.H., Saenko, O.A., Swingedouw, D., Sullivan, A., Yin, J., 2016. Fate of the Atlantic meridional overturning circulation: strong decline under continued warming and Greenland melting. Geophys. Res. Lett. 43, 12,252–12,260.
Balco, G., 2017. Production rate calculations for cosmic-ray-muon-produced ^{10}Be and ^{26}Al benchmarked against geological calibration data. Quat. Geochronol. 39, 150–173 (2017).
Balco, G., Stone, J., Lifton, N., Dunai, T.J., 2008. A simple, internally consistent, and easily accessible means of calculating surface exposure ages and erosion rates from Be-10 and Al-26 measurements. Quat. Geochronol. 3, 174–195.
Balco, G., Briner, J., Finkel, R.C., Rayburn, J.A., Ridge, J.C., Schaefer, J.M., 2009. Regional beryllium-10 production rate calibration for northeastern North America. Quat. Geochronol. 4, 93–107.
Barber, D.C., Dyke, A., Hillaire-Marcel, C., Jennings, A.E., Andrews, J.T., Kerwin, M.W., Bilodeau, G., McNeely, R., Southon, J., Morehead, M.D., Morgan, J.-M., 1999. Forcing of the cold event of 8,200 years ago by catastrophic drainage of Laurentide lakes. Nature 400, 344–348.
Bennike, O., Björck, S., 2002. Chronology of the last recession of the Greenland ice sheet. J. Quat. Sci. 17, 211–219.
Bennike, B., Wagner, B., Richter, A., 2011. Relative sea level changes during the Holocene in the Sisimiut area, south-western Greenland. J. Quat. Sci. 26, 353–361.
Bjørk, A.A., Kjær, K.H., Korsgaard, N.J., Khan, S.A., Kjeldsen, K.K., Andresen, C.S., Box, J.E., Larsen, N.K., Funder, S., 2012. An aerial view of 80 years of climate-related glacier fluctuations in southeast Greenland. Nat. Geosci. 5, 427–432.
Blaauw, M., Christen, J.A., 2011. Flexible paleoclimate age-depth models using an autoregressive gamma process. Bayesian Anal. 6, 457–474.
Bond, G., Showers, W., Cheseby, M., Lotti, R., Almasi, P., deMenocal, P., Priore, P., Cullen, H., Hajda, I., Bonani, G., 1997. A pervasive millennial-scale cycle in North Atlantic Holocene and glacial climates. Science 278, 1257–1266.
Böning, C.W., Behrens, E., Biastoch, A., Getzlaff, K., Bamber, J., 2016. Emerging impact of Greenland meltwater on deepwater formation in the North Atlantic Ocean. Nat. Geosci. 9, 523–527.
Briner, J.P., Miller, G.H., Davis, P.T., Finkel, R.C., 2006. Cosmogenic radionuclides from fiord landscapes support differential erosion by overriding ice sheets. GSA Bulletin 118, 406–420.
Briner, J.P., Overeem, I., Miller, G., Finkel, R.C., 2007. The deglaciation of clyde inlet, northeastern Baffin Island, Arctic Canada. J. Quat. Sci. 22, 223–232.
Briner, J.P., Davis, P.T., Miller, G.H., 2009. Latest pleistocene and Holocene glaciation of Baffin Island, Arctic Canada: key patterns and chronologies. Quat. Sci. Rev. 28, 2075–2087.
Briner, J.P., Young, N.E., Goehring, B.M., Schaefer, J.M., 2012. Constraining Holocene ^{10}Be production rates in Greenland. J. Quat. Sci. 27, 2–6.
Briner, J.P., Svendsen, J.I., Mangerud, J., Lohne, O.S., Young, N.E., 2014. A ^{10}Be chronology of south-western Scandinavian Ice Sheet history during the Lateglacial period. J. Quat. Sci. 29, 370–380.
Briner, J.P., McKay, N.P., Axford, Y., Bennike, O., Bradley, R.S., de Vernal, A., Fisher, D., Francus, P., Fréchette, B., Gajewski, K., Jennings, A., Kaufman, D.S., Miller, G., Rouston, C., Wagner, B., 2016. Holocene climate change in Arctic Canada and Greenland. Quat. Sci. Rev. 147, 340–364.
Bromley, G., Putnam, A., Borns Jr., H., Lowell, T., Sandford, T., Barrell, D., 2018. Interstadial rise and Younger Dryas demise of Scotland's last ice fields. Paleoceanography Paleoclimatol. 33, 412–429.
Buizert, C., Gkinis, V., Severnghaus, J.P., He, F., Lecavalier, B.S., Kindler, P., Meuenberger, M., Carlson, A.E., Vinther, B., Masson-Delmotte, V., White, J.W.C., Liu, Z., Otto-Bliesner, B., Brook, E.J., 2014. Greenland temperature response to climate forcing during the last deglaciation. Science 345, 1177–1180.
Carlson, A.E., Winsor, K., Ullman, D.J., Brook, E.J., Rood, D.H., Axford, Y., LeGrande, A.N., Anslow, F.S., Sinclair, G., 2014. Earliest Holocene south

Greenland ice sheet retreat within its late Holocene extent. Geograph. Res. Lett. 41 https://doi.org/10.1002/2014GL060800.
Carrivick, J.L., Yde, J., Russell, A.J., Quincey, D.J., Ingeman-Nielsen, T., Mallalieu, J., 2017. Ice-margin and meltwater dynamics during the mid-Holocene in the Kangerlussuaq area of west Greenland. Boreas 46, 369–387.
Clark, P.U., Marshall, S.J., Clarke, G.K.C., Hostetler, S.W., Licciardi, J.M., Teller, J.T., 2001. Freshwater forcing of abrupt climate change during the last glaciation. Science 293, 283–287.
Clark, P.U., Delworth, T.L., Weaver, A.J., 2008. Freshwater forcing: will history repeat itself? Science 320, 316–317.
Clark, P.U., Dyke, A.S., Shakun, J.D., Carlson, A.E., Clark, J., Wohlfarth, B., Mitrovica, J.X., Hostetler, S.W., Marshall McCabe, A., 2009. The last glacial maximum. Science 325, 710–714.
Clarke, G.K.C., Leverington, D.W., Teller, J.T., Dyke, A.S., 2004. Paleohydraulics of the last outburst flood from glacial Lake Agassiz and the 8200 BP cold event. Quat. Sci. Rev. 23, 389–407.
Condron, A., Winsor, P., 2011. A subtropical fate awaited freshwater discharged from glacial Lake Agassiz. Geophys. Res. Lett. 38, L03705. https://doi.org/10.1029/2010GL046011.
De Angelis, H., Kleman, J., 2007. Palaeo-ice streams in the foxe/baffin sector of the Laurentide ice sheet. Quat. Sci. Rev. 26, 1313–1331.
Denton, G.H., Alley, R.B., Comer, G.C., Broecker, W.S., 2005. The role of seasonality in abrupt climate change. Quat. Sci. Rev. 24, 1159–1182.
Dyke, A.S., 2004. An outline of North American deglaciation with emphasis on central and northern Canada. In: Ehlers, J., Gibbard, P.L. (Eds.), Developments in Quaternary Science, vol. 2. Elsevier), pp. 373–424.
Dykoski, C.A., Edwards, L.A., Cheng, H., Yuan, D., Cai, Y., Zhang, M., Lin, Y., Qing, J., An, Z., Revenaugh, J., 2005. A high-resolution, absolute-dated Holocene and deglacial Asian monsoon record from Dongge Cave, China. Earth Planet. Sci. Lett. 233, 71–86.
Falconer, G., Andrews, J.T., Ives, J.D., 1965. Late-Wisconsin end moraines in Northern Canada. Science 147, 608–610.
Feng, X., Yang, Y., Cheng, H., Zhao, J., Kong, X., Zhang, P., He, Z., Shi, X., Edwards, R.L., 2019. The 7.2 ka climate event: evidence from high-resolution stable isotopes and trace element records of stalagmite in Shuiming Cave, Chongqing, China. Holocene. https://doi.org/10.1177/0959683619875809.
Fleitmann, D., Mudelsee, M., Burns, S.J., Bradley, R.S., Kramers, J., Matter, A., 2008. Paleoceanography 23, PA1102. https://doi.org/10.1029/2007PA001519.
Funder, S., Hansen, L., 1996. The Greenland ice sheet – a model for its culmination and decay during and after the last glacial maximum. Bull. Geol. Soc. Den. 42, 137–152.
Funder, S., Kjellerup, K., Kjær, K.H., Ó Cofaigh, C., 2011. The Greenland ice sheet during the last 300,000 years: a review. In: Ehlers, J., Gibbard, P., Hughes, P.D. (Eds.), Quaternary Glaciations—Extent and Chronology: A Closer Look: Developments in Quaternary.
Garde, A.A., Marker, M., 2010. Geological Map of Greenland, 1:500 000, Søndre Strømfjord – Nuussuaq. Geological Survey of Denmark and Greenland, Copenhagen.
Granger, D.E., Lifton, N.A., Willenbring, J.K., 2013. A cosmic trip: 25 years of cosmogenic nuclides in geology. GSA Bulletin 125, 1379–1402.
Jennings, A., Andrews, J., Pearce, C., Wilson, L., Olfasdotttir, S., 2015. Detrital carbonate peaks on the Labrador shelf, a 13-7 ka template for freshwater forcing from the Hudson Strait outlet of the Laurentide Ice Sheet into the subpolar gyre. Quat. Sci. Rev. 107, 62–80.
Jóhannesson, T., Raymond, C., Waddington, E., 1989. Time-scale for adjustment of glaciers to changes in mass balance. J. Glaciol. 35, 355–369.
Kaplan, M.R., Miller, G.H., 2003. Early Holocene delevelling and deglaciation of the Cumberland sound region, Baffin Island, Arctic Canada. GSA Bulletin 115, 445–462.
Kelley, S.E., Briner, J.P., Young, N.E., Babonis, G.S., Csatho, B., 2012. Maximum late Holocene extent of the western Greenland Ice Sheet during the late 20th century. Quat. Sci. Rev. 56, 89–98.
Kelly, M.A., Lowell, T.V., Hall, B.L., Schaefer, J.M., Finkel, R.C., Goehring, B.M., Alley, R.B., Denton, G.H., 2008. A ^{10}Be chronology of lateglacial and Holocene mountain glaciation in the Scoresby Sund region, east Greenland: implications for seasonality during lateglacial time. Quat. Sci. Rev. 27, 2273–2282.
Kobashi, T., Menviel, L., Jeltsch-Thömmes, A., Vinther, B.M., Box, J.E., Muscheler, R., Nakaegawa, T., Pfister, P.L., Döring, M., Leuenberger, M., Wanner, H., Ohmura, A., 2017. Volcanic influence on centennial to millennial Holocene Greenland temperature change. Sci. Rep. 7, 1441. https://doi.org/10.1038/s41598-017-0451-7.
Lal, D., 1991. Cosmic ray labeling of erosion surfaces: in situ nuclide production rates and erosion models. Earth Planet. Sci. Lett. 104, 424–429.
LeGrande, A.N., Schmidt, G.A., 2008. Ensemble, water isotope-enabled, coupled general circulation modeling insights into the 8.2 ka event. Paleoceanography 23, PA3207. https://doi.org/10.1029/2008PA001610.
LeGrande, A.N., Schmidt, G.A., Shindell, D.T., Field, C.V., Miller, R.L., Koch, D.M., Faluvegi, G., Hoffmann, G., 2006. Consistent simulations of multiple proxy responses to an abrupt climate change event. Proc. Natl. Acad. Sci. U.S.A. 103, 837–842. https://doi.org/10.1073/pnas.0510095103.
Lesnek, A.J., Briner, J.P., 2018. Response of a land-terminating sector of the western Greenland Ice Sheet to early Holocene climate change: evidence from ^{10}Be dating in the Søndre Isortoq region. Quat. Sci. Rev. 180, 145–156.
Levy, L.B., Kelly, M.A., Howley, J.A., Virginia, R.A., 2012. Age of the ørkendalen moraines, Kangerlussuaq, Greenland: constraints on the extent of the southwestern margin of the Greenland ice sheet during the Holocene. Quat. Sci. Rev. 52, 1–5.
Levy, L.B., Kelly, M.A., Lowell, T.V., Hall, B.L., Howley, J.A., Smith, C.A., 2016. Coeval fluctuations of the Greenland ice sheet and a local glacier, central East Greenland, during late glacial and early Holocene time. Geophys. Res. Lett. 43, 1623–1631.
Levy, L.B., Kelly, M.A., Applegate, P.A., Howley, J.A., Virginia, R.A., 2018. Middle to late Holocene chronology of the western margin of the Greenland Ice Sheet: a comparison with Holocene temperature and precipitation records. Arct. Anarct. Alp. Res. 50, e1414477.
Licciardi, J.M., Teller, J.T., Clark, P.U., 1999. Freshwater routing by the Laurentide ice sheet during the last deglaciation. In: Clark, P.U., Webb, R.S., Keigwin, L.D. (Eds.), Mechanisms of Global Climate Change at Millennial Time Scales. American Geophysical Union, Washington, DC, pp. 177–201.
Long, A.J., Roberts, D.H., Dawson, S., 2006. Early Holocene history of the west Greenland ice sheet and GH-8.2 event. Quat. Sci. Rev. 25, 904–922.
Lowell, T.V., Hayward, R.K., Denton, G.H., 1999. Role of climate oscillations in determining ice- margin positions: hypothesis, examples, implications. In: Mickelson, D.M., Attig, J.W. (Eds.), Glacial Processes Past and Present. Geological Society of America Special, Boulder, CO. Paper 337.
MacAyeal, D.R., 1993. Binge/purge oscillations of the Laurentide ice sheet as a cause of the north Atlantic's heinrich events. Paleoceanography 8, 775–784.
Mangerud, J., Aarseth, I., Hughes, A.C., Lohne, Ø.S., Skår, K., Sønstegaard, E., Svendsen, J.I., 2016. A major re-growth of the scandinavian ice sheet in western Norway during Allerød-younger Dryas. Quat. Sci. Rev. 132, 175–205.
McKay, N.P., Emile-Geay, J., 2016. Technical note: the Linked Paleo Data framework – a common tongue for paleoclimatology. Clim. Past 12, 1093–1100.
McKay, N.P., Emile-Geay, J., Heiser, C., Khider, D., 2018. GeoChronR development repository. https://doi.org/10.5281/zenodo. 60812.
Miller, G.H., 1973. Late quaternary glacial and climatic history of northern Cumberland Peninsula, Baffin Island, N.W.T., Canada. Quat. Res. 3, 561–583.
Miller, G.H., Wolfe, A.P., Steig, E.J., Sauer, P.E., Kaplan, M.R., Briner, J.P., 2002. The Goldilocks dilemma: big ice, little ice or "just-right" ice in the Eastern Canadian Arctic. Quat. Sci. Rev. 21, 33–48.
Morrill, C., Ward, E.M., Wagner, A.J., Otto-Bliesner, B.L., Rosenbloom, N., 2014. Large sensitivity to freshwater forcing location in 8.2 ka simulations. Paleoceanography 29. https://doi.org/10.1002/2014PA002669.
Nishiizumi, K., Imamura, M., Caffee, M.W., Southon, J.R., Finkel, R.C., McAninch, J., 2007. Absolute calibration of ^{10}Be AMS standards. Nucl. Instrum. Methods Phys. Res. B 258, 403–413.
Ó Cofaigh, C., Dowdeswell, J.A., Jennings, A.E., Hogan, K.A., Kilfeather, A., Hiemstra, J.F., Noormets, R., Evans, J., McCarthy, D.J., Andrews, J.T., Lloyd, J.M., Moros, M., 2013. An extensive and dynamic ice sheet on the West Greenland shelf during the last glacial cycle. Geology 41, 219–222.
Oerlemans, J., 2005. Extracting a climate signal from 169 glacier records. Science 308, 675–677.
O'Hara, S.L., Briner, J.P., Kelley, S.E., 2017. A ^{10}Be chronology of early Holocene local glacier moraines in central West Greenland. Boreas 46, 655–666.
Pearce, C., Andrews, J.T., Bouloubassi, I., Hillaire-Marcel, C., Jennings, A.E., Olsen, J., Kuijpers, A., Seidenkrantz, M.-S., 2015. Heinrich 0 on the east Canadian margin: source, distribution, and timing. Paleoceanography 30, 1613–1624.
Pendleton, S., Miller, G., Lifton, N., Young, N., 2019. Cryosphere response resolves conflicting evidence for the timing of peak Holocene warmth on Baffin Island, Arctic Canada. Quat. Sci. Rev. 216, 107–115.
Putnam, A., et al., 2019. *In situ*^{10} Be production-rate calibration from a ^{14}C-dated late-glacial moraine belt in Rannoch Moor, central Scottish Highlands. Quaternary Geochronology 50, 109–125.
Rahmstorf, S., Box, J.E., Feulner, G., Mann, M.E., Robinson, A., Rutherford, S., Schaffernicht, E.J., 2015. Exceptional twentieth-century slowdown in Atlantic Ocean overturning circulation. Nat. Clim. Chang. 5, 475–480.
Rainsley, E., Menviel, L., Fogwill, C.J., Turney, C.S.M., Hughes, A.L.C., Rood, D.H., 2018. Greenland ice mass loss during the younger Dryas driven by Atlantic meridional overturning circulation feedbacks. Sci. Rep. 8, 11307.
Rasmussen, S.O., Anderson, K.K., Svensson, A.M., Steffensen, J.P., Vinther, B.M., Clausen, H.B., Siggaard-Andersen, M.-L., Johnsen, S.J., Larsen, L.B., Dahl-Jensen, D., Bigler, M., Röthlisberger, R., Fischer, H., Goto-Azuma, K., Hansson, M.E., Ruth, U., 2006. A new Greenland ice core chronology for the last glacial termination. J. Geophys. Res. 111, D06102.
Rasmussen, S.O., Vinther, B.M., Clausen, H.B., Andersen, K.K., 2007. Early Holocene climate oscillations recorded in three Greenland ice cores. Quat. Sci. Rev. 26, 1907–1914.
Reimer, P.J., Bard, E., Bayliss, A., Beck, J.W., Blackwell, P.G., Ramsey, C.B., Buck, C.E., Cheng, H., Edwards, R.L., Friedrich, M., Grootes, P.M., Guilderson, T.G., Haflidason, H., Hajdas, I., Hatté, C., Heaton, T.J., Hoffmann, D.L., Hogg, A.G., Hughen, K.A., Kaiser, K.F., Kromer, B., Manning, S.W., Niu, M., Reimer, R.W., Richards, D.A., Scott, E.M., Southon, J.R., Staff, R.A., Turney, C.S.M., van der Plicht, J., 2013. Intcal13 and Marine13 radiocarbon age calibration curves 0-50,000 Years cal bp. Radiocarbon 55, 1869–1887.
Renssen, H., Seppä, H., Heiri, O., Roche, D.M., Goosse, H., Fichefet, T., 2009. The spatial and temporal complexity of the Holocene thermal maximum. Nat. Geosci. 2, 411–414.
Rinterknecht, V., Gorokhovich, Y., Schaefer, J., Caffee, M., 2009. Preliminary ^{10}Be chronology for the last deglaciation of the western margin of the Greenland Ice Sheet. J. Quat. Sci. 24, 270–278.
Roberts, D.H., Long, A.J., Schnabel, C., Davies, B.J., Xu, S., Simpson, M.J.R., Huybrechts, P., 2009. Ice Sheet extent and early deglacial history of the

southwestern sector of the Greenland Ice Sheet. Quat. Sci. Rev. 28, 2670–2773.
Robinson, A., Calov, R., Ganopolski, A., 2012. Multistability and critical thresholds of the Greenland ice sheet. Nat. Clim. Chang. 2, 429–432.
Roe, G.H., 2011. What do glaciers tell us about climate variability and climate change? 2011. J. Glaciol. 57, 567–578.
Roe, G.H., O'Neal, M.A., 2009. The response of glaciers to intrinsic climate variability: observations and models of late-Holocene variations in the Pacific Northwest. J. Glaciol. 55, 839–854.
Roe, G.H., Baker, M.B., Herla, F., 2017. Centennial glacier retreat as categorical evidence of regional climate change. Nat. Geosci. 10, 95–99.
Schaefer, J.M., Denton, G.H., Kaplan, M., Putnam, A., Finkel, R.C., Barrell, D.J.A., Andersen, B.G., Schwartz, R., Mackintosh, A., Chinn, T., Schlüchter, C., 2009. High-frequency Holocene glacier fluctuations in New Zealand differ from the Northern signature. Science 324, 622–625.
Seidenkrantz, M.-S., Ebbesen, H., Aagaard-Sørensen, S., Moros, M., Lloyd, J.M., Olsen, J., Knudsen, M.F., Kuijpers, A., 2013. Early Holocene large-scale meltwater discharge from Greenland documented by foraminifera and sediment parameters. Palaeogeogr. Palaeoclimatol. Palaeoecol. 391, 71–81.
Sodemann, H., Schwierz, C., Wernli, H., 2008. Interannual variability of Greenland winter precipitation sources: Lagrangian moisture diagnostic and North Atlantic Oscillation influence. J. Geophys. Res. Atmos. 113, D03107.
Staiger, J., Gosse, J., Toracinta, R., Oglesby, B., Fastook, J., Johnson, J.V., 2007. Atmospheric scaling of cosmogenic nuclide production: climate effect. J. Geophys. Res. 112, B02205.
Stone, J.O., 2000. Air pressure and cosmogenic isotope production. J. Geophys. Res. 105, 23,753-23,759.
Ten Brink, N.W., 1975. Holocene history of the Greenland Ice Sheet based on radiocarbon- dated moraines in west Greenland. Meddelelser om Grønland 44, 113pp.
Thomas, E.R., Wolff, E.W., Mulvaney, R., Steffensen, J.P., Johnsen, S.J., Arrowsmith, C., White, J.W.C., Vaughn, B., Popp, T., 2007. The 8.2 ka event from Greenland ice cores. Quat. Sci. Rev. 26, 70–81.
Thomas, E.K., Castañeda, I.S., McKay, N.P., Briner, J.P., Salacup, J.M., Nguyen, K.Q., Schweinsberg, A.D., 2018. A wetter Arctic coincident with hemispheric warming 8,000 years ago. Geograph. Res. Lett. 45 https://doi.org/10.1029/2018GL079517.
Thornalley, D.J.R., Elderfield, H., McCave, N., 2009. Holocene oscillations in temperature and salinity of the surface subpolar North Atlantic. Nature 457, 711–714.
Thornalley, D.J.R., Oppo, D.W., Ortega, P., Robson, J.I., Brierley, C.M., Davis, R., Hall, I.R., Moffa-Sanchez, P., Rose, N.L., Spooner, P.T., Yashayaev, I., Keigwin, L.D., 2018. Anomalously weak Labrador Sea convection and Atlantic overturning during the past 150 years. Nature 556, 227–230.
Ullman, D.J., Carlson, A.E., Hostetler, S.W., Clark, P.U., Cuzzone, J., Milne, G.A., Winsor, K., Caffee, M., 2016. Final Laurentide ice-sheet deglaciation and Holocene climate-sea level change. Quat. Sci. Rev. 152, 49–59.
Vacco, D.A., Alley, R.B., Pollard, D., 2009. Modeling dependence of moraine deposition on climate history: the effect of seasonality. Quat. Sci. Rev. 128, 639–646.
van Tatenhove, F.G., van der Meer, J.J., Koster, E.A., 1996. Implications for deglaciation chronology from new AMS age determinations in central West Greenland. Quat. Res. 45, 245–253.
Wagner, A.J., Morrill, C., Otto-Bliesner, B.L., Rosenbloom, N., Watkins, K.R., 2013. Model support for forcing of the 8.2 ka event by meltwater from the Hudson Bay ice dome. Clim. Dyn. 41, 2855–2873.
Weidick, A., 1968. Observations on some Holocene glacier fluctua- tions in West Greenland. Meddelelser Om Grønland 165, 1–202.
Weidick, A., 1974. Quaternary Map of Greenland, 1:500 000, Søndre Strømfjord – Nûgssuaq. Copenhagen. Geological Survey of Greenland.
Wheeler, J.O., Hoffman, P.F., Card, K.D., Davidson, A., Sanford, B.V., Okulitch, A.V., Roest, W.R., 1997. Geological Map of Canada. Geological Survey of Canada. Map 1860A.
Winsor, K., Carlson, A.E., Caffee, M.W., Rood, D.H., 2015. Rapid last-deglacial thinning and retreat of the marine-terminating southwestern Greenland ice sheet. Earth Planet. Sci. Lett. 426, 1–12.
Young, N.E., Briner, J.P., Axford, Y., Csatho, B., Babonis, G.S., Rood, D.H., Finkel, R.C., 2011. Response of a marine-terminating Greenland outlet glacier to abrupt cooling 8200 and 9300 years ago. Geophs. Res. Lett. 38, L24701. https://doi.org/10.1029/2011GL049639.
Young, N.E., Briner, J.P., Rood, D.H., Finkel, R.C., 2012. Glacier extent during the younger Dryas and 8.2-ka event on Baffin Island, Arctic Canada. Science 337, 1330–1333.
Young, N.E., Briner, J.P., Maurer, J., Schaefer, J., 2016. ^{10}Be measurements in bedrock constrain erosion beneath the Greenland Ice Sheet margin. Geophys. Res. Lett. 43 https://doi.org/10.1002/2016GL070258.
Young, N.E., Briner, J.P., Rood, D.H., Finkel, R.C., Corbett, L.B., Bierman, P.R., 2013b. Age of the Fjord Stade moraines in the Disko Bugt region, western Greenland, and the 9.3 and 8.2 ka cooling events. Quat. Sci. Rev. 60, 76–90.
Young, N.E., Briner, J.P., Schaefer, J., Zimmerman, S., Finkel, R.C., 2019. Early Younger Dryas glacier culmination in southern Alaska: implications for North Atlantic climate change during the last deglaciation. Geology 47, 550–554.
Young, N.E., Schaefer, J.M., Briner, J.P., Goehring, B.M., 2013a. A ^{10}Be production-rate calibration for the Arctic. J. Quat. Sci. 28, 515–526.
Yu, S.-Y., Colman, S.M., Lowell, T.V., Milne, G.A., Fisher, T.G., Breckenridge, A., Boyd, M., Teller, J.T., 2010. Freshwater outburst from Lake Superior as a trigger for the cold event 9300 years ago. Science 328, 1262–1266.